Hammerhead-type FXR agonists induce an eRNA *FincoR* that ameliorates nonalcoholic steatohepatitis in mice

Jinjing Chen[a, #], Ruoyu Wang[b, #], Feng Xiong[b], Hao Sun[a], Byron Kemper[a], Wenbo Li[b,*] and Jongsook Kim Kemper[a,*]

[a]Department of Molecular and Integrative Physiology, University of Illinois at Urbana-Champaign, Urbana, IL, USA and [b]Department of Biochemistry and Molecular Biology, McGovern Medical School, University of Texas Health Science Center, Houston, TX, USA

Running Title: Role of an FXR-induced eRNA, *FincoR*, in NASH

[#]JC and RW contributed equally to this study.

Present Address: Jinjing Chen, Department of Pharmacology and Toxicology, University of Arizona, Tucson, AZ, USA

* To whom correspondence may be addressed:

* Wenbo Li, Department of Biochemistry and Molecular Biology, McGovern Medical School, University of Texas Health Science Center, Houston, TX, USA

Tel: 713-500-6103, e-mail: Wenbo.Li@uth.tmc.edu

* J. Kim Kemper, Department of Molecular and Integrative Physiology,

University of Illinois at Urbana-Champaign, Urbana, IL

Tel: 217-722-7961, e-mail: jongsook@illinois.edu

Key words: FXR, nuclear receptor, lncRNA, enhancer, enhancer RNA, tropifexor, hepatic inflammation, NASH, NAFLD, RNA-seq, Gro-seq

Author Contributions:

JC, RW, WL and JK designed research; JC, RW, WL, FX, and HS performed experiments; RW and WL performed bioinformatic analyses; JC, RW, WL, and BK analyzed data; and JC, RW, BK, WL, and JK wrote the paper.

Abstract

The nuclear receptor, Farnesoid X Receptor (FXR/NR1H4), is increasingly recognized as a promising drug target for metabolic diseases, including nonalcoholic steatohepatitis (NASH). Protein coding genes regulated by FXR are well known, but whether FXR also acts through regulation of long non-coding RNAs (lncRNAs), which vastly outnumber protein-coding genes, remains unknown. Utilizing RNA-seq and GRO-seq analyses in mouse liver, we found that FXR activation affects the expression of many RNA transcripts from chromatin regions bearing enhancer features. Among these we discovered a previously unannotated liver-enriched enhancer-derived lncRNA (eRNA), termed *FincoR*. We show that *FincoR* is specifically induced by the hammerhead-type FXR agonists, including GW4064 and tropifexor. CRISPR/Cas9-mediated liver-specific knockdown of *FincoR* in dietary NASH mice reduced the beneficial effects of tropifexor, an FXR agonist currently in clinical trials for NASH and primary biliary cholangitis (PBC), indicating that that amelioration of liver fibrosis and inflammation in NASH treatment by tropifexor is mediated in part by *FincoR*. Overall, our findings highlight that pharmacological activation of FXR by hammerhead-type agonists induces a novel eRNA, *FincoR*, contributing to the amelioration of NASH in mice. *FincoR* may represent a new drug target for addressing metabolic disorders, including NASH.

67 **Introduction**

68 Nonalcoholic fatty liver disease (NAFLD) is the most common chronic liver disease and
69 a leading cause of liver transplants and liver-related death *(Friedman et al., 2018)*. NAFLD
70 begins with simple steatosis but may further progress to a severe form, non-alcoholic
71 steatohepatitis (NASH), and later, fatal cirrhosis and liver cancer *(Friedman et al., 2018)*.
72 Despite its striking global increase and clinical importance, there is no approved drug for
73 NASH. The urgent need for development of therapeutic agents for NASH has greatly
74 increased research interest in the nuclear receptor, Farnesoid X Receptor (FXR, NR1H4)
75 *(Evans & Mangelsdorf, 2014)*.

76 FXR is activated by its physiological ligands, bile acids (BAs), and regulates
77 expression of genes involved in BA, lipid, and glucose metabolism and hepatic autophagy,
78 which maintain metabolite levels and metabolic homeostasis *(Calkin & Tontonoz, 2012;*
79 *Kliewer & Mangelsdorf, 2015; Lee et al., 2006; Lee et al., 2014; Seok et al., 2014)*. Ligand-
80 activated FXR also protects against hepatic inflammation and liver injury *(Jung et al.,*
81 *2020; Wang et al., 2008)*. The action of FXR, similar to other nuclear receptors, is
82 achieved primarily by its binding to chromatin loci to regulate the transcription of target
83 genes *(Calkin & Tontonoz, 2012; Lee et al., 2006; Lee et al., 2012; Thomas et al., 2010)*.
84 Consistent with its crucial physiological functions, FXR is increasingly recognized as a
85 promising drug target, particularly for liver diseases, such as NASH and primary biliary
86 cholangitis (PBC) *(Abenavoli et al., 2018; Ali et al., 2015; Downes et al., 2003; Kremoser,*
87 *2021)*. For example, semi-synthetic or non-steroidal synthetic agonists of FXR, including
88 obeticholic acid (OCA) and hammerhead-type agonists, such as tropifexor and cilofexor,
89 are currently in clinical trials for NASH and PBC patients *(Abenavoli et al., 2018; Kremoser,*

90 *2021; Sanyal et al., 2023; Tully et al., 2017)*. However, how pharmacological activation of
91 FXR mediates such beneficial therapeutic effects is poorly understood.

92 Non-protein-coding RNAs (ncRNAs) are one of the fascinating discoveries of
93 modern biology *(Cech & Steitz, 2014)*. While a significant portion of the genome was
94 initially thought to be "junk DNA", it has been established that many non-coding regions
95 give rise to functional non-coding RNAs *(Cech & Steitz, 2014)*. Of these ncRNAs, long
96 non-coding RNAs (lncRNAs) are a group of transcripts longer than 200 nucleotides and
97 play important roles in diverse biological processes *(Lam et al., 2014; Li et al., 2016;*
98 *Mattick et al., 2023; Sartorelli & Lauberth, 2020; Statello et al., 2021)*. A group of lncRNAs
99 are produced from genomic regions bearing epigenetic features of enhancers *(Hon et al.,*
100 *2017; Mattick et al., 2023)*. This is consistent with the idea that many transcriptional
101 enhancers actively transcribe noncoding RNAs that are referred to as eRNAs (>85k in
102 humans and >57k in mice) *(Hirabayashi et al., 2019)*, some of which are functionally
103 important for enhancer functions *(Lai & Shiekhattar, 2014; Li et al., 2016; Sartorelli &*
104 *Lauberth, 2020)*. A majority of eRNAs have not yet been annotated in current lncRNA
105 databases, such as GENCODE. Exploring eRNA landscapes and functions in diverse
106 biology and disease states will facilitate our understanding of both lncRNAs and
107 enhancers *(Li et al., 2016; Mattick et al., 2023)*. Indeed, the landscape of eRNAs in mouse
108 liver has been minimally explored *(Fang et al., 2014)*, and has not been well-studied in
109 response to specific nuclear receptor activation, such as by FXR. Moreover, functional
110 roles of eRNAs *in vivo* in intact organisms is understudied.

111 FXR was shown to regulate expression of small non-coding microRNA (miR)
112 genes, for example *miR-34a and miR-802 (Lee et al., 2010; Seok et al., 2021)*, but it has

113 not been reported whether FXR achieves its function through regulating lncRNAs, which
114 far outnumber miRs. Because FXR directly regulates expression of its target genes *(Lee*
115 *et al., 2012; Thomas et al., 2010)*, we examined if FXR regulates enhancer-derived
116 lncRNAs (eRNAs), and if such transcripts participate in its physiological or
117 pharmacological functions. By utilizing RNA-seq and GRO-seq analyses of livers from
118 mice treated with FXR ligands, we identified a set of FXR-regulated eRNAs. Among these,
119 we focused on a highly induced and abundantly expressed eRNA that we referred to as
120 FXR-induced non-coding RNA (*FincoR*) for functional studies. *FincoR* is highly enriched
121 in mouse liver and is induced specifically by hammerhead-type FXR agonists, including
122 GW4064 and tropifexor. *In vivo* studies utilizing CRISPR/Cas9-mediated liver-specific
123 knockdown of *FincoR* in dietary NASH mice indicated that *FincoR* is critically involved in
124 mediating the beneficial pharmacological effects of tropifexor in reducing liver fibrosis and
125 inflammation.
126
127 **Results**
128 **Activation of FXR by GW4064 induces a novel eRNA, *FincoR*, in mouse liver**
129 To identify enhancer-derived lncRNAs (eRNAs) potentially regulated by FXR, we first
130 obtained a list of putative enhancers in mouse liver based on ENCODE H3K27ac ChIP-
131 Seq data (ENCFF001KMI, see **methods**). Then, we performed ribo-depleted total RNA-
132 seq in the livers from mice treated with a specific FXR agonist, GW4064, to identify
133 transcripts produced from these enhancer regions (see **Supplementary Table S1**). To
134 avoid confounding issues of RNA signals from genes, we specifically focused on

135 intergenic enhancer regions (+/- 3kb from H3K27ac peak center) that harbor discernible
136 RNA-Seq signals (RPKM > 1).

137 This genomic analysis resulted in identification of 190 high-confidence eRNAs in
138 mouse liver. Among these, 14 eRNAs were upregulated and 5 were downregulated by
139 GW4064 treatment (FDR < 0.05, Log2 FC > 1, **Figure 1A**) (see **Supplementary Table**
140 **S2**). FXR-regulated eRNAs were produced adjacent to many genes with important roles
141 in liver metabolism and disease, for example, *Hes1* (**Figure 1-figure supplement 1A, B**).
142 One of the most robustly induced eRNAs was *FXR-induced non-coding RNA* (*FincoR)*,
143 an unannotated novel transcript located on chromosome 19 (**Figure 1A, B, C**). Reverse
144 transcription qPCR (RT-qPCR) confirmed that treatment with GW4064 substantially
145 induced expression of *FincoR,* more than 10-fold in mouse liver, which is similar to
146 induction of *Shp*, a well-known FXR target gene (**Figure 1D**) *(Claudel et al., 2005; Evans*
147 *& Mangelsdorf, 2014; Goodwin et al., 2000)*. Induction of *FincoR* by GW4064 was
148 transient, peaked within 1 h and then declined gradually, a pattern similar to that of *Shp*
149 (**Figure 1-figure supplement 1C**). Expression of genes adjacent to *FincoR*, including
150 *Gcnt1, Rfk, Pcsk5 and Prune2,* did not change after acute 1 h FXR activation as shown
151 by RNA-seq (**Figure 1C**), and confirmed for *Gcnt1* by time course qPCR (**Figure 1-figure**
152 **supplement 1C**).

153 We also found that the short-time GW4064 treatment resulted in 590 up-regulated
154 genes and 500 down-regulated genes (FDR < 0.05) (**Figure 1-figure supplement 2A**).
155 GO enrichment analysis of these differentially expressed genes (DEGs) revealed their
156 roles in the regulation of triglyceride, fatty acid, and cholesterol metabolism (**Figure 1-**

157 **figure supplement 2B**), which is consistent with known roles of FXR in these
158 physiological processes *(Claudel et al., 2005)*.
159
160 **Ligand-activated FXR directly activates transcription of eRNAs, including *FincoR***
161 We sought to examine, 1) if these eRNAs were directly activated by FXR, and 2) if the
162 activation takes place transcriptionally using FXR liver-specific knockout (FXR-LKO) mice
163 that were treated with GW4064 to determine if FXR was required for induction of eRNAs
164 by GW4064. FXR-LKO mice were generated from FXR floxed mice (FXR-flox) **(Figure 2-**
165 **figure supplement 1A**) and transcription of eRNAs was detected by global run-on
166 sequencing (GRO-seq), a widely used method to detect nascent RNA transcription,
167 including eRNAs *(Lam et al., 2014; Li et al., 2016; Sartorelli & Lauberth, 2020)*. GRO-seq
168 showed that FXR-induced eRNAs were activated transcriptionally by GW4064 in FXR-
169 flox mice, but such induction was abolished in FXR-LKO mice (**Figure 2A**). In particular,
170 *FincoR* is robustly induced in the GRO-Seq analysis and its induction is dependent on
171 hepatic FXR (**Figure 2B**). RT-qPCR confirmed the FXR-dependent expression of *FincoR,*
172 similar to that of *Shp* (**Figure 2-figure supplement 1B**).
173 We next examined if FXR binds to the enhancers that produce the identified
174 eRNAs by analyzing published mouse liver ChIP-Seq data for FXR (**Supplementary**
175 **Table S3**) *(Lee et al., 2012; Thomas et al., 2010)*. FXR binding was strongly enriched at
176 the enhancers associated with FXR-induced eRNAs as were the enhancer marks
177 H3K27ac and H3K4me1 (**Figure 2-figure supplement 1C**). The binding of FXR and the
178 presence of histone marks at the *FincoR* enhancer region determined by ChIP-seq as
179 compared with nascent transcripts detected by Gro-seq is shown in **Figure 2B**. These

180 analyses support the conclusion that activation of FXR transcriptionally induces this
181 series of eRNAs via chromatin binding at these enhancers, including *FincoR*.

182 We validated FXR binding at the enhancer region that produces *FincoR* using
183 mouse liver ChIP (**Figure 2C**). We also examined binding of a well-known DNA binding
184 partner of FXR, Retinoid x Receptor alpha (RXRα/NR2B1) *(Evans & Mangelsdorf, 2014;*
185 *Zheng et al., 2018)*, and bromodomain-containing protein 4 (BRD4), an acetylated histone
186 reader protein that often binds at active enhancers *(Chen et al., 2016; Li et al., 2016;*
187 *Rahnamoun et al., 2018; Sartorelli & Lauberth, 2020)* and is a transcriptional coactivator
188 of FXR *(Jung et al., 2020)*. GW4064 treatment resulted in substantial increases in
189 recruitment of both FXR and RXRα to the enhancer region close to the transcription start
190 site of *FincoR* (arrow shown below in Figure 2B), whereas binding was not detected at a
191 control region (**Figure 2C**). We also found that BRD4 occupancy was increased at this
192 enhancer region after GW4064 treatment (**Figure 2C**). These results indicate that
193 GW4064 activation of FXR leads to increased occupancy of the FXR/RXRα heterodimer
194 and BRD4 to the enhancer region to upregulate *FincoR* eRNA in the liver.

195 We identified an inverted repeat1 (IR1) motif that is known to bind FXR *(Calkin &*
196 *Tontonoz, 2012; Lee et al., 2006)* within the major FXR binding peak near the start site of
197 *FincoR* (arrow shown below in Figure 2B), which we also refer to as FXRE (**Figure 2B,**
198 **C**). We examined the functionality of this IR1 motif for mediating transcriptional activation
199 by GW4064 using reporter assays (**Figure 2D**). We cloned the region containing the IR1
200 motif into the pGL4.23 luciferase reporter and generated a mutated IR1 motif construct
201 as a comparison (**Figure 2D**). After transfection into human hepatic HepG2 cells,
202 GW4064 treatment significantly elevated the luciferase activity of the reporter with the

203 wild type IR1 motif, but not with the mutated IR1 motif (**Figure 2D**). Together, these results
204 suggest that GW4064-activated FXR directly upregulates *FincoR* expression.
205
206 ***FincoR* is a liver-specific nucleus-enriched eRNA**
207 Because enhancers and eRNAs generally act in a tissue-specific manner *(Li et al., 2016;*
208 *Sartorelli & Lauberth, 2020)*, we examined the tissue-specific expression of *FincoR* in
209 mice. Strikingly, *FincoR* is highly expressed in the liver and it is expressed at extremely
210 low levels in most other tissues, except for a detectable, but still fairly low, level in the
211 lung (**Figure 3A**). GW4064 treatment resulted in induction of *FincoR* specifically in the
212 liver (**Figure 3A**). The level of *FincoR* detected in primary mouse hepatocytes (PMHs)
213 isolated from GW4064-treated mouse liver was similar to that in the liver tissue from the
214 same mouse, suggesting that the majority of *FincoR* is present in hepatocytes (**Figure**
215 **3B**).
216 By using the 5' and 3' rapid amplification of cDNA ends (RACE), we identified one
217 transcript of *FincoR* that is of approximately 3.7 kb in length (**Figure 3C**). However, based
218 on RNA-seq, the length of *FincoR* is over 10 kb (**Figure 1C**), suggesting there are likely
219 additional multiple RNA isoforms that we were not able to identify by RACE. We next
220 analyzed the coding potential of *FincoR* utilizing a comparative genomic program,
221 PhyloCSF. While adjacent genes *Gcnt1* and *Prune2* (**Figure 3D, E**) were correctly
222 predicted to encode proteins, *FincoR* did not contain a potential protein-coding open
223 reading frame (**Figure 3E**). Consistent with this bioinformatic prediction, a vector
224 expressing *FincoR* failed to produce any proteins in an in vitro transcription/translation
225 assay (**Figure 3F**) confirming that the *FincoR* transcript is a noncoding RNA. *FincoR*

226 transcripts were enriched by binding to oligo-dT beads, suggesting that *FincoR* is 3'
227 polyadenylated (**Figure 3G**). Further, *FincoR* was detected in the nuclear compartment
228 and GW4064 treatment increased the nuclear abundance of *FincoR* (**Figure 3H**),
229 consistent with its potential transcriptional regulatory function. Together, these results
230 from molecular biochemical characterization studies reveal that *FincoR* is a liver-enriched
231 nuclear polyadenylated eRNA.
232
233 ***FincoR* is induced specifically by the hammerhead-type synthetic FXR agonists**
234 To determine whether induction of the FXR-induced *FincoR* is ligand-specific, we
235 examined the effects of several hammerhead-type synthetic FXR agonists, including
236 GW4064, cilofexor, and tropifexor; a semi-synthetic agonist, OCA; and a non-
237 hammerhead-type gut-specific agonist, fexaramine (**Figure 4A**) *(Downes et al., 2003;*
238 *Fang et al., 2015)*. Remarkably, treatment with each of the hammerhead type agonists
239 for 1 h resulted in a robust induction of *FincoR* (**Figure 4B**), whereas *FincoR* levels were
240 unchanged after treatment with OCA or fexaramine for 1 h (**Figure 4B**). Treatment with
241 OCA for 4 h or even one-week treatment with OCA failed to induce hepatic *FincoR* in
242 mice, while expression of *Shp* was significantly induced (**Figure 4C, D**). Acute feeding
243 with a diet supplemented with 0.5% cholic acid (CA), a primary BA, for 6 h also failed to
244 induce *FincoR* expression (**Figure 4E**). Collectively, these results demonstrate that
245 *FincoR* is induced specifically by hammerhead-type FXR agonists.
246
247 **Generation of CRISPR/Cas9-mediated *FincoR* liver-specific knockdown mice**

248 To explore the functional role of hepatic FincoR, we utilized the CRISPR/Cas9 technique
249 to generate *FincoR* liver-specific knockdown (FincoR-LKD) mice (**Figure 5-figure**
250 **supplement 1A, B**). Adenoviral-mediated sgRNA expression in Cas9 mice resulted in
251 downregulation of *FincoR* specifically in the liver by about 60%, but not in other tissues
252 (**Figure 5B**). As FXR is a key regulator of bile acid, cholesterol, lipid, and glucose
253 metabolism and *FincoR* is specifically regulated by FXR, *FincoR* may have a role in the
254 metabolic process in physiology and disease. We examined liver triglyceride, cholesterol,
255 bile acid, glycogen and serum non-esterified fatty acids (NEFA) but *FincoR*
256 downregulation did not result in any significant changes under physiological conditions
257 (**Figure 5C**).

258 To explore the molecular signatures and pathways affected by FincoR, we
259 examined global gene expression by RNA-seq analysis in mouse liver after *FincoR*
260 knock-down (**Figure 5D**). While *FincoR* was markedly downregulated, the neighboring
261 genes, such as *Gcnt1, Rfk, Pcsk5 and Prune2*, were largely unchanged (**Figure 5D;**
262 **Figure 5-figure supplement 1C**). The RNA-seq analysis revealed 18 up-regulated genes
263 and 53 downregulated genes in FincoR-LKD liver (**Supplementary Table S4; Figure 5E**).
264 GO analysis of those downregulated genes indicated that these genes were enriched in
265 pathways involved in fatty acid oxidation, organelle organization and metabolic process
266 (**Figure 5F**). Among the down-regulated genes, *Ppp1r3g,* which has a role in controlling
267 glycogen synthesis, and *Igfbp2,* which functions in insulin resistance, were markedly
268 reduced (**Supplementary Table S4; Figure 5-figure supplement 1D, E**). Among the up-
269 regulated genes, expression was substantially increased for *Eda2r*, which is a member
270 of the tumor necrosis factor receptor superfamily and is involved in inflammation, the

271 immune response, and development (**Figure 5-figure supplement 1F**). *Fndc1,* which is
272 involved in fibronectin matrix remodeling, was also suppressed by *FincoR* (and thus
273 upregulated upon its KO, **Figure 5-figure supplement 1G**). These studies suggest that
274 *FincoR* has a role in modulating metabolic homeostasis by regulating genes involved in
275 metabolism and inflammation.
276
277 **Amelioration of hepatic steatosis mediated by tropifexor is independent of *FincoR***
278 **in diet-induced NASH mice**
279 Tropifexor, also known as LJN452, is a highly potent hammerhead type FXR agonist that
280 is currently under clinical trials for NASH and PBC patients *(Kremoser, 2021; Sanyal et*
281 *al., 2023; Tully et al., 2017)*. Because *FincoR* is induced specifically by the hammerhead
282 class of FXR agonist (**Figure 4**) and has a potential role in the regulation of metabolism
283 and inflammation (**Figure 5**), we hypothesized that *FincoR* may play a role in tropifexor-
284 mediated beneficial effects on reducing NASH pathologies in mice.
285 We utilized a mouse model that had been fed the Amylin Liver NASH-promoting
286 (AMLN) diet *(Hernandez et al., 2019; Sun et al., 2022; Zhao et al., 2018)*, and examined
287 the potential impact of liver-specific downregulation of *FincoR* on tropifexor's effects on
288 NASH pathology. Cas9 mice fed the AMLN diet for 12 weeks were injected via tail veins
289 with adenovirus expressing control sgRNA or *FincoR* sgRNA, respectively, and then
290 treated daily with tropifexor (0.3 mg/kg) for 12 days (**Figure 6A**). In these mice, as a
291 technical validation of RNA induction and knockdown, *FincoR* levels were significantly
292 increased by FXR agonist tropifexor, and the increase was blocked by adenovirus
293 expressing sgRNA for *FincoR* (**Figure 6B**).

294 We then examined the effect of tropifexor treatment and *FincoR* downregulation
295 on hepatic steatosis in these mice. Tropifexor treatment markedly reduced neutral lipids
296 determined by Oil Red O staining of liver sections (**Figure 6C**) and liver TG levels (**Figure**
297 **6D**), and these beneficial effects on reducing fatty liver were not altered by *FincoR*
298 downregulation. Also, *FincoR* downregulation had little effect on liver cholesterol and
299 gallbladder BA levels, although gallbladder BA levels were reduced by tropifexor (**Figure**
300 **6D**).

301 Consistent with the phenotypes, hepatic expression of key genes involved in BA
302 synthesis was dramatically reduced by tropifexor treatment (i.e., *Cyp7a1 and Cyp8b1*),
303 which is consistent with decreased gallbladder BA levels mediated by this agonist (**Figure**
304 **6E**). Similarly, tropifexor also lowered lipid synthesis genes (*Srebp1c, Lpin1*, *Scd1*),
305 consistent with decreased liver TG levels. However, downregulation of *FincoR* did not
306 result in changes in mRNA levels of these genes (**Figure 6E**). These results indicate that
307 tropifexor-mediated beneficial effects on reducing hepatic steatosis are independent of
308 *FincoR*.

309

310 ***FincoR* facilitates alleviation of liver inflammation by tropifexor in diet-induced**
311 **NASH**

312 Tropifexor ameliorated fibrotic NASH pathologies in preclinical studies *(Hernandez et al.,*
313 *2019; Tully et al., 2017)* and has recently concluded phase 2 clinical trials for NASH
314 patients *(Sanyal et al., 2023)*. We, therefore, further examined the effects of *FincoR*
315 downregulation on altering other NASH pathologies, including hepatocellular apoptosis,
316 liver fibrosis and inflammation.

317 In the same AMLN diet-fed mice as described above (**Figure 6**), analyses of liver
318 sections revealed that tropifexor treatment reduced hepatocyte swelling/ballooning (H&E
319 staining), decreased numbers of apoptotic cells (TUNEL staining), alleviated fibrosis
320 (Sirius red staining), and lowered infiltration of macrophages (F4/80 staining) (**Figure 7A**).
321 Remarkably, these tropifexor-mediated beneficial effects on NASH pathologies were all
322 markedly diminished by *FincoR* downregulation (**Figure 7A**). This was consistently found
323 in various liver lobes and two representative pictures from two different lobes are shown
324 (**Figure 7A**). In control experiments, *FincoR* downregulation in vehicle-treated mice did
325 not result in marked changes in NASH pathologies (**Figure 7-figure supplement 1**).
326 These results demonstrate that *FincoR* is required for tropifexor-mediated beneficial
327 effects on reducing NASH pathologies, specifically reducing hepatic inflammation, fibrosis
328 and hepatocyte apoptosis. Consistent with these results, serum ALT and AST levels,
329 indicators of liver damage, were significantly elevated after *FincoR* downregulation
330 (**Figure 7B**). Protein levels of key inflammatory markers, IL1β and CCL2, in liver extracts
331 were also elevated after *FincoR* downregulation (**Figure 7C**).

332 Consistent with the phenotypes from histological analyses, hepatic expression of
333 fibrosis and inflammation was altered by *FincoR* knockdown. For example, tropifexor
334 treatment reduced mRNA levels of several genes that promote fibrosis (*Col1a1, Col1a2,*
335 *Acta2*) and hepatic inflammation (*Eda2r, Ifng, Ccl3)*, whereas these reductions were
336 largely reversed by *FincoR* downregulation (**Figure 7D**). We also detected increased
337 expression of inflammatory genes (*Ccl2, Ccr2, Lcn2)* and an extracellular matrix
338 remodeling gene *(Fndc1)* in liver with *FincoR* knockdown (**Figure 7D**). Tropifexor
339 treatment suppresses hepatic apoptosis by reducing pro-apoptotic genes (*Ctsb, Ctss*)

340 and upregulating anti-apoptotic genes such as *Bcl2 (Warren et al., 2019)*. Importantly,
341 these effects were significantly reversed by *FincoR* downregulation (**Figure 7D**).
342 Collectively, these results demonstrate that in diet-induced NASH mice,
343 pharmacological activation of FXR by tropifexor reduced fibrosis, apoptosis, and
344 inflammation, which was dependent, at least in part, on the induction of *FincoR*.
345
346 ***FincoR* expression is increased in chronic liver disease with hepatic inflammation**
347 **and liver injury**
348 To determine whether expression of *FincoR* is altered in chronic liver disease, we utilized
349 mouse models of NAFLD/NASH and cholestatic liver injury. Hepatic *FincoR* levels were
350 significantly increased in mice fed with a high fat diet (HFD) for 12 weeks
351 (**Supplementary Figure S1A**) and in mice fed a HFD with high fructose (HFHF) in
352 drinking water for 12 weeks (**Supplementary Figure S1B**). Elevated hepatic *FincoR*
353 levels were also observed in mice treated with α-naphthylisothiocyanate (ANIT), a
354 chemical inducer of liver cholestasis *(Jung et al., 2020; Kim et al., 2016)* (**Supplementary**
355 **Figure S1C**), and in mice with bile duct ligation (BDL), a surgical method to induce
356 cholestatic liver injury (**Supplementary Figure S1D**).
357 The sequence of *FincoR* is moderately conserved between mice and humans as
358 displayed in the UCSC genome browser (**Supplementary Figure S1E**). Annotation in the
359 NCBI genome data viewer of the human sequence region with similarity to mouse *FincoR*
360 revealed an functionally uncharacterized human lncRNA, XR_007061585.1, in this region
361 **(Supplementary Figure S1F)**. However, whether this sequence (or an as yet to be
362 identified lncRNA) is functional or not has not been determined. To explore the potential

363 changes or role of lncRNA XR_007061585.1 in human liver pathological conditions, we
364 measured hepatic levels of the transcripts in PBC and NAFLD patients. Compared to
365 normal individuals, hepatic lncRNA XR_007061585.1 levels were elevated in patients
366 with PBC or NAFLD, but not in severe NASH-fibrosis patients (**Supplementary Figure**
367 **S1G, H**). These results demonstrate that hepatic levels of a potential human analog of
368 *FincoR* are elevated in NAFLD and PBC patients, as *FincoR* is in mouse models of
369 chronic liver disease with hepatic inflammation and liver injury. However, whether human
370 lncRNA XR_007061585.1 is analogous to mouse *FincoR* in terms of functions and
371 mechanisms, and whether elevated XR_007061585.1 levels may have a role in the
372 disease progression or may be an adaptive response to liver injury remains to be
373 determined.
374

375 **Discussion**

376 FXR maintains metabolic homeostasis by transcriptional regulation of genes. Direct
377 regulation of protein-coding genes by FXR, including *Shp*, is well characterized. In this
378 study we show that FXR also mediates its functions by induction of lncRNA genes, which
379 vastly outnumber protein-coding genes. We further show that pharmacological activation
380 of FXR by hammerhead-type agonists induces a liver-specific enhancer-derived lncRNA,
381 which we named *FincoR*, that contributes to reduction of NASH pathologies in mice.

382 *FincoR* is specifically induced by the hammerhead class of FXR agonists, such as
383 GW4064, cilofexor, and tropifexor. GW4064 is the mother compound of these isoxazole-
384 type hammerhead ligands but is not an ideal therapeutic agent because of its poor water
385 solubility and pharmacokinetics *(Abel et al., 2010)*. In contrast, tropifexor and cilofexor

386 have better pharmacokinetics and are generally well-tolerated in clinical trials for NASH
387 and PBC patients *(Abenavoli et al., 2018; Kremoser, 2021; Sanyal et al., 2023; Tully et*
388 *al., 2017)*, but the underlying mechanisms for their beneficial effects are poorly
389 understood. Intriguingly, a recent study showed that the gene signature regulated by
390 tropifexor-activated FXR appears to be broader than that of OCA, partly because the
391 tropifexor backbone allows a more favorable interaction of FXR with coactivators or
392 epigenomic modulators *(Hernandez et al., 2019)*. Further, tropifexor was shown to
393 regulate distinct sets of genes in experimental NASH as compared to other FXR agonists,
394 particularly genes involved in fibrosis, inflammation, and oxidative stress *(Hernandez et*
395 *al., 2019)*. Utilizing CRISPR/Cas9-mediated liver-specific knockdown of *FincoR* in diet-
396 induced NASH mice, we demonstrate that beneficial effects on reducing liver fibrosis,
397 inflammation, and apoptosis mediated by tropifexor were largely dependent on *FincoR*
398 (Model, **Figure 7E**).

399 While this study focused on regulation of *FincoR* by pharmacological activation of
400 FXR, physiological and pathological regulations of *FincoR* appear to be complex.
401 Although *FincoR* can be induced by the hammerhead class of FXR agonists, it was not
402 induced by the endogenous FXR ligand, cholic acid. This implies that *FincoR* may not
403 contribute to the physiological functions of FXR. In an effort to investigate the potential
404 role of FincoR in the pathological conditions, we observed that *FincoR* levels were
405 elevated in mouse models of cholestasis and NASH as well as in human PBC and NAFLD
406 patients, where BA metabolism is dysregulated. Since different BAs can activate or
407 repress the gene-regulating function of FXR *(Wahlstrom et al., 2016)*, altered BA
408 composition in these pathological conditions may contribute to induction of *FincoR*.

409 Further, binding peaks for multiple nuclear receptors, FXR, LXR, PPARα, RXRα, and
410 HNF-4α, were detected in the *FincoR* locus so that regulation of *FincoR* likely involves
411 the combinatorial regulation by multiple nuclear receptors (**Supplementary Figure S2**).
412 Interestingly, occupancy of the nuclear receptor PPARα at the enhancer region was
413 increased in fasted mice (**Supplementary Figure S3**). It will be interesting to investigate
414 whether and how *FincoR* is differently regulated by these nuclear receptors in response
415 to physiological and pathological cues.

416 The roles of regulatory RNAs in liver function and diseases and their potentials as
417 therapeutic targets are increasingly being appreciated *(Brocker et al., 2020; Li et al., 2021;*
418 *Sallam et al., 2016; Zhao et al., 2018)*. For example, a critical role for an oxysterol nuclear
419 receptor LXR-induced lncRNA, *LeXis*, in feedback modulation of cholesterol biosynthesis
420 has been shown *(Sallam et al., 2016)*. Recently, the role of a lncRNA, *Pair*, in liver
421 phenylalanine metabolism has been demonstrated *(Li et al., 2021)*. Enhancer RNAs are
422 a less characterized class of lncRNAs and are highly associated with enhancer functions
423 in gene regulation *(Li et al., 2016)*. Numerous studies have revealed transcriptional roles
424 for eRNAs in various cellular processes *(Lai & Shiekhattar, 2014; Lam et al., 2014; Li et*
425 *al., 2016; Sartorelli & Lauberth, 2020)* but most previous eRNA studies have used
426 cultured cells *(Hsieh et al., 2014; Li et al., 2013)*, with only a few *in vivo* studies in mouse
427 models *(Mirtschink et al., 2019; Tang et al., 2023)*. In our current study, through integrative
428 analysis of transcriptome and histone mark ChIP-Seq, we identified a group of FXR-
429 regulated eRNAs, including the highly induced *FincoR*. Our current work characterized
430 the role of *FincoR* in gene regulation and in mediating beneficial pharmacological effects
431 of tropifexor in NASH, representing important progress in understanding the roles of

432 eRNAs *in vivo*. Future work is warranted to elucidate the exact mechanisms by which
433 *FincoR* facilitates action of FXR agonists to alleviate inflammation, fibrosis and apoptosis.
434 RNA inside the cells usually associates with different RNA-binding proteins (RBPs)
435 *(Gerstberger et al., 2014)*. We identified potential binding proteins of *FincoR* using the
436 ATtRACT database (*Giudice et al., 2016*). The top four candidates for *FincoR* binding are
437 KHDRBS1, RBM38, YBX2 and YBX3 (**Supplemental Table S5**). KHDRBS1 and RBM38
438 have been reported to have important roles in RNA processing (*Bielli et al., 2011; Zou et*
439 *al., 2021*). YBX2 and YBX3 belong to the Y-box (YBX) protein family, which have been
440 linked to diverse forms of RNA metabolism and many other processes, including cell
441 proliferation, DNA repair, stress responses, development, and inflammation (*Kleene,*
442 *2018*). Whether these predicted RBPs interact with *FincoR* and how they contribute to
443 phenotypes should be investigated in future experimentation to understand the
444 mechanisms involved in *FincoR*-regulated hepatocyte function.
445 There is limitation of some of our approaches that cannot fully dissect the
446 underlying mechanisms of *FincoR*. Currently, the function of eRNA loci can be attributed
447 to a functional eRNA transcript, or binding of transcription factors to this region, or the
448 transcription process itself, or some combination of these effects *(Li et al., 2016; Sartorelli*
449 *& Lauberth, 2020)*. In our studies to decrease expression of *FincoR*, the region containing
450 the FXR binding site was deleted (**Figure 5-figure supplement 1A, right panel**). While
451 the expression of *FincoR* transcripts was significantly reduced, we cannot rule out
452 whether decreased binding of FXR or decreased transcription contribute to the observed
453 changes in phenotype. To directly investigate the function of *FincoR* transcripts,

454 downregulation of the transcript with antisense oligonucleotides together with
455 overexpression of *FincoR* in the liver will be required in future experiments.
456 FXR is increasingly recognized as an important therapeutic target for
457 enterohepatic diseases, but the development of clinically applicable and more targeted
458 FXR-based therapy is still challenging. In this study, we provided the first characterization
459 of an eRNA, *FincoR*, induced by pharmacological activation of FXR and show that *FincoR*
460 has a beneficial role in reducing liver fibrosis and inflammation in dietary NASH mice.
461 Complete understanding of the function and mechanisms of *FincoR* may provide novel
462 insights for the development of desirable therapy for NASH and other chronic liver
463 diseases.
464

465 **Materials and Methods**

466 **Animal experiments**

467 All animal studies were performed according to procedures approved by the Institutional
468 Animal Care & Use Committee at the University of Illinois at Urbana-Champaign and were
469 in accordance with National Institutes of Health guidelines. Mice were maintained in
470 12/12 h light/dark cycles and fed standard rodent chow. FXR-LKO mice were generated
471 by breeding FXR floxed mice with Albumin-Cre mice (The Jackson Lab). *FincoR*-LKD
472 mice were generated as previously reported *(Zhao et al., 2018)*. Briefly, Cas9 transgenic
473 mice (JAX #024858) were injected via the tail vein with adenoviruses (approximately
474 $5x10^8$ PFU) expressing two sgRNAs targeting *FincoR* (sgRNA1:
475 *GGGTTAAGAGCTGTAGGCTG* and sgRNA2: ACTTCTATGTCCAACAACCG). The
476 sequences of sgRNAs were designed using a CRISPR design tool (http://crispr.mit.edu/).

477 Mice were given a single dose of vehicle or 30 mg/kg GW4064 (in corn oil, Tocris
478 Bioscience, #2473) after overnight fasting. Mice were treated with 0.5 mg/kg tropifexor (in
479 corn oil, MedChem Express, HY-107418), 30 mg/kg cilofexor (in corn oil,
480 MedChemExpress, HY-109083), 100 mg/kg fexaramine (in 0.5% methylcellulose,
481 MedChem Express, HY-10912), and 20 mg/kg OCA (in 0.5% methylcellulose, MedChem
482 Express, HY-12222) as indicated. C57BL6 mice were fed with a chow diet containing
483 0.5% CA for 6 h *(Jung et al., 2020)*.

484 To induce cholestasis, mice were treated by gavage with 75 mg/kg α-naphthyl
485 isothiocyanate (ANIT) for 48 hours as previously reported *(Jung et al., 2020; Kim et al.,*
486 *2016; Kim et al., 2020)*. Cholestasis was also induced by bile duct ligation or sham
487 operation in mice for 24 hours or 72 hours *(Li et al., 2018)*.

488 To induce dietary obesity, mice were fed a high-fat diet (TD88137; Harlan Teklad)
489 or a high-fat diet with 25% fructose in water (high fat/high fructose) for 12 weeks *(Seok et*
490 *al., 2021)*.

491 To investigate the effect of liver-specific downregulation of *FincoR* on NASH, male
492 Cas9 mice were fed the AMLN diet (Research Diets, D09100310, 40 kcal% fat, 2%
493 cholesterol, 20 kcal% fructose) for 12 weeks and then, were injected with adenovirus
494 expressing control sgRNA or sgRNA targeting FincoR. Administration of tropifexor was
495 started 3 days later and given at 0.3 mg/kg dissolved in corn oil.

496

497 **RNA-Seq**

498 C57BL/6 mice were fasted overnight and *i.p.* injected with vehicle or GW4064 (30 mg/kg)
499 for 1 h, and livers were collected (n = 4 mice for either vehicle or treated group). Total

500 RNA from each liver was extracted by RNeasy kit (Qiagen), and two randomly selected
501 mice liver RNAs were pooled for RNA-seq (two RNA-seq reactions from 4 mice livers for
502 either vehicle or treated group). RNA-seq was performed as previously described *(Byun*
503 *et al., 2018; Byun et al., 2020; Seok et al., 2018)*. Ribosomal RNA was removed with the
504 Ribozero HMR Gold kit (Illumina). The sequencing library was generated following
505 methods described below.
506
507 **Construction of strand-specific RNAseq libraries**
508 Construction of the RNAseq libraries and sequencing on the Illumina NovaSeq 6000 were
509 performed at the Roy J. Carver Biotechnology Center at the University of Illinois at
510 Urbana-Champaign. After DNase digestion, purified total RNAs were analyzed on a
511 Fragment Analyzer (Agilent) to evaluate RNA integrity. The total RNAs were converted
512 into individually barcoded polyadenylated mRNAseq libraries with the Kapa HyperPrep
513 mRNA kit (Roche). Libraries were barcoded with Unique Dual Indexes (UDI's) which have
514 been developed to prevent index switching. The adaptor-ligated double-stranded cDNAs
515 were amplified by PCR for 8 cycles with the Kapa HiFi polymerase (Roche). The final
516 libraries were quantitated with Qubit (Thermo Fisher) and the average cDNA fragment
517 sizes were determined on a Fragment Analyzer. The libraries were diluted to 10 nM and
518 further quantitated by qPCR on a CFX Connect Real-Time qPCR system (Bio-Rad) for
519 accurate pooling of barcoded libraries and maximization of number of clusters in the
520 flowcell.
521
522 **Sequencing of libraries in the NovaSeq**

523 The barcoded RNAseq libraries were loaded on one SP lane on a NovaSeq 6000 for
524 cluster formation and sequencing. The libraries were sequenced from one end of the
525 fragments for a total of 100 bp. The fastq read files were generated and demultiplexed
526 with the bcl2fastq v2.20 Conversion Software (Illumina, San Diego, CA). The quality of
527 the demultiplexed fastq files was evaluated with the FastQC software, which generates
528 reports with the quality scores, base composition, k-mer, GC and N contents, sequence
529 duplication levels and overrepresented sequences.
530
531 **GRO-seq**
532 To harvest the nuclei from mouse liver cells, the liver was harvested at indicated time and
533 washed with a cold swelling buffer (10 mM Tris-HCl, pH 7.5, 2 mM $MgCl_2$, 3 mM $CaCl_2$,
534 2 U/ml Superase-In). The nuclei were prepared by Dounce homogenization in cold
535 swelling buffer and filtered using a cell strainer (100 μm, BD Biosciences). Nuclei were
536 collected by centrifugation at 400 x g for 10 min, then resuspended in the lysis buffer
537 (swelling buffer with 10% glycerol and 1% IGEPAL) and incubated on ice for 5 min. Nuclei
538 were washed twice with the lysis buffer and resuspended at a concentration of 10^8
539 nuclei/ml in the freezing buffer (50 mM Tris-HCl, pH 8.3, 40% glycerol, 5 mM $MgCl_2$, 0.1
540 mM EDTA). We then followed our previous method *(Li et al., 2013; Oh et al., 2021)* to
541 conduct nuclear run-on and GRO-Seq library preparation. Briefly, the nuclei in freezing
542 buffer were subjected to the nuclear run-on reaction by mixing with an equal volume of
543 run-on buffer (10 mM Tris-HCl, pH 8.0, 5 mM $MgCl_2$, 1 mM dithiothreitol (DTT), 300 mM
544 KCl, 20 units of Superase-In, 1% sarkosyl, 500 μM ATP, GTP, Br-UTP and 2 μM CTP) for
545 5 min at 30 °C. The BrU-labeled run-on RNAs were extracted by TRIzol and purified by

546 anti-BrdU agarose beads (Santa Cruz Biotech, sc-32323 AC). The run-on RNAs were
547 then subjected to end repair by T4 PNK, poly-adenylation, and then to cDNA first strand
548 synthesis by a custom primer (oNTI223) that allows circularization of the cDNA. This
549 cDNA then was re-linearized by Ape1 (NEB), size selected by TBE gel electrophoresis
550 and the products of the desired size were excised (~320–350 bp) for final library prep and
551 sequencing. GRO-Seq samples were run on a NextSeq 500 sequencer from Illumina with
552 a single-end 80 nt model.
553
554 **Histological analyses**
555 For histology, tissues were dissected and immediately fixed in 10% formalin overnight
556 and processed for paraffin embedding and H&E staining. Paraffin-embedded liver
557 sections were incubated with F4/80 antibody, and antibody was detected using a
558 peroxidase-based method (Abcam, ab64238). Liver collagen was detected by Sirius Red
559 staining (Abcam, ab246832) and apoptosis was detected by TUNEL staining (Millipore,
560 S7100). For Oil Red O staining, liver tissue was frozen in OCT compound (Sakura
561 Finetek, 4583), sectioned, and stained. Liver sections were imaged with a NanoZoomer
562 Scanner (Hamamatsu) and quantification was done using NIH ImageJ.
563
564 **Metabolic analyses**
565 Hepatic levels of TG (Sigma, MAK266), cholesterol (Sigma, MAK043), glycogen
566 (Biovision, K646-100), total BA levels (Diazyme, DZ042A), serum NEFA (Sigma,
567 MAK044), serum ALT (Sigma, MAK052) and serum AST (Sigma, MAK055) were
568 determined according to the manufacturer's instructions. Mouse liver IL-1β (R&D

569 systems, MLB00C) and CCL2 (R&D systems, DY479-05) were detected by commercially
570 available ELISA kit.
571
572 **Liver samples of PBC and NAFLD patients.** Liver specimens from normal organ
573 donors, and patients with PBC or NAFLD were obtained from the Liver Tissue
574 Procurement and Distribution System. The samples were unidentifiable, and thus, ethical
575 approval was not required. Hepatic XR_007061585.1 levels were measured by qPCR.
576
577 **Mouse liver ChIP**
578 Liver ChIP assay was performed as described previously *(Jung et al., 2020; Seok et al.,*
579 *2018)*. Briefly, chromatin extracts were prepared from FXR floxed and FXR-LKO mouse
580 livers after treatment of the mice with GW4064 which was followed by preclearing and
581 immunoprecipitation using control IgG or FXR antibody (Novus Biologicals, NBP2-16550;
582 Santa Cruz, sc-25309), RXRα antibody (Proteintech, catalog no. 21218-1-AP), or BRD4
583 antibody (Bethyl Laboratories, catalog #A301-985A50). Enrichment in chromatin
584 precipitates of gene sequences was measured by qRCR using primers listed
585 (**Supplementary Table S6**).
586
587 **Primary mouse hepatocytes and HepG2 cells**
588 Primary hepatocytes were isolated from C57BL/6 mice by collagenase (Worthington
589 Biochemical Corporation, LS004188) perfusion and maintained in William's E Medium
590 with primary hepatocyte maintenance supplements (Gibco #CM4000) in six-well plates

591 as described previously *(Jung et al., 2020; Kim et al., 2015)*. HepG2 cells were maintained
592 in DMEM supplemented with 10% fetal bovine serum at 37°C and 5% CO_2.
593
594 **Luciferase reporter assay**
595 The enhancer region containing the FXR binding element was amplified by PCR and
596 cloned into the pGL4.23 vector (Promega). HepG2 cells were transiently transfected with
597 FXR (100 ng/well) and RXRα (5 ng/well) in combination with reporters containing the wild
598 type FXRE or mutated FXRE (200 ng/well) (**Supplementary Table S6**). β-galactosidase
599 plasmid (200 ng/well) was also transfected as an internal control. Cells were treated with
600 GW4064 or DMSO after transient transfection. Six hours later, the cells were harvested.
601 All reporter assays were repeated at least three times in triplicates.
602
603 **RACE**
604 5' and 3' RACE assays were performed using a SMARTer RACE kit (Clontech) according
605 to the manufacturer's instructions. The resulting PCR products were separated by
606 electrophoresis in agarose gels and cloned into the pRACE vector provided by the kit.
607 The transcription start sites and end sites of *FincoR* were determined by sequencing. The
608 gene-specific primers used for 5'- and 3'-RACE are listed in **Supplementary Table S6**.
609
610 **In vitro transcription and translation (TNT)**
611 Expression plasmids for luciferase and *FincoR* were mixed with a Coupled Reticulocyte
612 Lysate System (Promega). After incubating at 30ºC for 60 min, translated products were
613 separated on 4-20% gradient SDS polyacrylamide gels and transferred to PVDF

614 membranes. Chemiluminescent detection of in vitro translated protein was performed
615 following the manufacturer's protocol (Promega).
616
617 **RT-qPCR**
618 Total RNA was extracted using the RNeasy Mini Kit (Qiagen, 74104) and 2 μg of RNA
619 was reverse transcribed and mRNA expression was normalized relative to that of 36B4.
620 The qPCR primers are shown in **Supplementary Table S6**.
621
622 **Subcellular fractionation**
623 Using a Cytoplasmic and Nuclear RNA Purification Kit (Norgen, Thorold, ON, Canada),
624 the cytoplasm and nucleus fractions from primary hepatocytes isolated from livers of mice
625 treated with GW4064 or DMSO were separated, and both fractions were subjected to
626 RNA extraction and qRT-PCR.
627
628 **Immunoblotting analysis**
629 Total liver lysates were prepared as described before *(Sun et al., 2022)*. Antibodies for
630 immunoblotting for β-ACTIN (#4970) were purchased from Cell Signaling Technology.
631 Antibodies for immunoblotting for FXR (sc-25309) were purchased from Santa Cruz.
632
633 ***FincoR* polyadenylation study**
634 Total RNA was prepared using the RNeasy mini prep kit (Qiagen). Poly(A)+ and poly(A)-
635 RNA was separated using a Dynabeads™ mRNA Purification Kit (ThermoFisher
636 Scientific) according to the manufacturer's instructions. Briefly, total RNA was incubated
637 with the Dynabeads/binding buffer suspension at room temperature for 5 min and the

638 reaction tubes were placed on a magnet until solution was clear. The supernatant
639 containing poly(A)- RNA was saved. The beads with poly(A)+ RNA were washed three
640 times with washing buffer provided by the kit. RNA was extracted from the supernatant
641 and beads respectively using Trizol. qPCR was performed to analyze levels of *FincoR*
642 and 36b4 in the poly(A)+ and poly(A)- RNA fractions.
643

644 **Genomics Analysis**

645 RNA-Seq and GRO-Seq reads were mapped to the mouse reference genome mm10 with
646 STAR aligner *(Dobin et al., 2013)*. Transcript quantifications were done with the HOMER
647 tool set *(Heinz et al., 2010)* and enhancer RNAs were identified based on H3K27ac ChIP-
648 Seq in mouse liver. Briefly, intergenic H3K27ac ChIP-Seq peaks were selected as
649 putative enhancer regions in mouse liver. Then +/- 3kb regions around putative
650 enhancers with RNA-Seq signal (>1 RPKM) were considered as putative eRNAs in
651 mouse livers. Overlapped eRNAs regions were merged, and redundant ones were
652 removed. In addition, any +/- 3kb extended eRNAs regions that overlapped with protein-
653 coding genes were further removed to avoid transcriptional readthrough from genes. We
654 used DESeq2 *(Love et al., 2014)* to identify significantly regulated eRNAs with a cutoff of
655 (FDR < 0.05, Log2FC > 1). Public ChIP-Seq datasets were obtained from ENCODE or
656 GEO (**Supplementary Table S3**).
657

658 **Statistical analysis**

659 Statistical analysis was performed using GraphPad Prism 9. Statistical differences were
660 evaluated using the two-tailed unpaired Student's t-test for comparisons between two

661 groups, or ANOVA and appropriate post hoc analyses for comparisons of more than two
662 groups. Statistical methods and corresponding *p* values for data shown in each panel are
663 indicated in figure legends.
664
665 **Data availability**
666 RNA-seq and Gro-seq data were deposited in GEO under the following accession
667 numbers GSE 221986.
668
669 **Acknowledgments**
670 We thank Deepa Prakashini Govindasamy Rajagopal for the help with tissue genotyping.
671 We thank Tiangang Li at University of Oklahoma for providing bile-duct ligated mouse
672 liver samples, and Kristina Schoonjans at Ecole Polytech, Switzerland, for providing FXR
673 floxed mice. We also thank the Liver Tissue Cell Distribution System, University of
674 Minnesota (NIH Contract # HHSN276201200017C), for providing liver specimens of
675 NAFLD and PBC patients and individuals without liver disease. This study was supported
676 by an American Diabetes Association Postdoctoral Fellowship to J.C. (1-19-PDF-117),
677 and by a John and Rebekah Harper Fellowship to R.W. W.L. is a Cancer Prevention and
678 Research Institute of Texas (CPRIT) Scholar (RR160083). This work is supported by
679 funding from NIH (K22CA204468 and R01GM136922), and Welch Foundation (AU-2000-
680 20220331) to W.L., and grants from the NIH (R01 DK062777 and R01 DK095842) to
681 J.K.K.
682

683 **References**

684 Abel, U., Schluter, T., Schulz, A., Hambruch, E., Steeneck, C., Hornberger, M.,
685 Hoffmann, T., Perovic-Ottstadt, S., Kinzel, O., Burnet, M., Deuschle, U., &
686 Kremoser, C. (2010). Synthesis and pharmacological validation of a novel series
687 of non-steroidal FXR agonists. *Bioorg Med Chem Lett*, *20*(16), 4911-4917.
688 https://doi.org/10.1016/j.bmcl.2010.06.084
689 Abenavoli, L., Falalyeyeva, T., Boccuto, L., Tsyryuk, O., & Kobyliak, N. (2018).
690 Obeticholic Acid: A New Era in the Treatment of Nonalcoholic Fatty Liver
691 Disease. *Pharmaceuticals (Basel)*, *11*(4). https://doi.org/10.3390/ph11040104
692 Ali, A. H., Carey, E. J., & Lindor, K. D. (2015). Recent advances in the development of
693 farnesoid X receptor agonists. *Ann Transl Med*, *3*(1), 5.
694 https://doi.org/10.3978/j.issn.2305-5839.2014.12.06
695 Bielli, P., Busa, R., Paronetto, M. P., & Sette, C. (2011). The RNA-binding protein
696 Sam68 is a multifunctional player in human cancer. *Endocr Relat Cancer*, *18*(4),
697 R91-R102. https://doi.org/10.1530/ERC-11-0041
698 Brocker, C. N., Kim, D., Melia, T., Karri, K., Velenosi, T. J., Takahashi, S., Aibara, D.,
699 Bonzo, J. A., Levi, M., Waxman, D. J., & Gonzalez, F. J. (2020). Long non-coding
700 RNA Gm15441 attenuates hepatic inflammasome activation in response to
701 PPARA agonism and fasting. *Nat Commun*, *11*(1), 5847.
702 https://doi.org/10.1038/s41467-020-19554-7
703 Byun, S., Kim, D. H., Ryerson, D., Kim, Y. C., Sun, H., Kong, B., Yau, P., Guo, G., Xu,
704 H. E., Kemper, B., & Kemper, J. K. (2018). Postprandial FGF19-induced
705 phosphorylation by Src is critical for FXR function in bile acid homeostasis. *Nat*
706 *Commun*, *9*(1), 2590. https://doi.org/10.1038/s41467-018-04697-5
707 Byun, S., Seok, S., Kim, Y. C., Zhang, Y., Yau, P., Iwamori, N., Xu, H. E., Ma, J.,
708 Kemper, B., & Kemper, J. K. (2020). Fasting-induced FGF21 signaling activates
709 hepatic autophagy and lipid degradation via JMJD3 histone demethylase. *Nat*
710 *Commun*, *11*(1), 807. https://doi.org/10.1038/s41467-020-14384-z
711 Calkin, A. C., & Tontonoz, P. (2012). Transcriptional integration of metabolism by the
712 nuclear sterol-activated receptors LXR and FXR. *Nat Rev Mol Cell Biol*, *13*(4),
713 213-224. https://doi.org/10.1038/nrm3312
714 Cech, T. R., & Steitz, J. A. (2014). The noncoding RNA revolution-trashing old rules to
715 forge new ones. *Cell*, *157*(1), 77-94. https://doi.org/10.1016/j.cell.2014.03.008
716 Chen, J., Wang, Z., Hu, X., Chen, R., Romero-Gallo, J., Peek, R. M., Jr., & Chen, L. F.
717 (2016). BET Inhibition Attenuates Helicobacter pylori-Induced Inflammatory
718 Response by Suppressing Inflammatory Gene Transcription and Enhancer
719 Activation. *J Immunol*, *196*(10), 4132-4142.
720 https://doi.org/10.4049/jimmunol.1502261
721 Claudel, T., Staels, B., & Kuipers, F. (2005). The Farnesoid X receptor: a molecular link
722 between bile acid and lipid and glucose metabolism. *Arterioscler Thromb Vasc*
723 *Biol*, *25*(10), 2020-2030. https://doi.org/10.1161/01.ATV.0000178994.21828.a7
724 Dobin, A., Davis, C. A., Schlesinger, F., Drenkow, J., Zaleski, C., Jha, S., Batut, P.,
725 Chaisson, M., & Gingeras, T. R. (2013). STAR: ultrafast universal RNA-seq
726 aligner. *Bioinformatics*, *29*(1), 15-21.
727 https://doi.org/10.1093/bioinformatics/bts635

728 Downes, M., Verdecia, M. A., Roecker, A. J., Hughes, R., Hogenesch, J. B., Kast-
729 Woelbern, H. R., Bowman, M. E., Ferrer, J. L., Anisfeld, A. M., Edwards, P. A.,
730 Rosenfeld, J. M., Alvarez, J. G., Noel, J. P., Nicolaou, K. C., & Evans, R. M.
731 (2003). A chemical, genetic, and structural analysis of the nuclear bile acid
732 receptor FXR. *Mol Cell*, *11*(4), 1079-1092. https://doi.org/10.1016/s1097-
733 2765(03)00104-7
734 Evans, R. M., & Mangelsdorf, D. J. (2014). Nuclear Receptors, RXR, and the Big Bang.
735 *Cell*, *157*(1), 255-266. https://doi.org/10.1016/j.cell.2014.03.012
736 Fang, B., Everett, L. J., Jager, J., Briggs, E., Armour, S. M., Feng, D., Roy, A., Gerhart-
737 Hines, Z., Sun, Z., & Lazar, M. A. (2014). Circadian enhancers coordinate
738 multiple phases of rhythmic gene transcription in vivo. *Cell*, *159*(5), 1140-1152.
739 https://doi.org/10.1016/j.cell.2014.10.022
740 Fang, S., Suh, J. M., Reilly, S. M., Yu, E., Osborn, O., Lackey, D., Yoshihara, E.,
741 Perino, A., Jacinto, S., Lukasheva, Y., Atkins, A. R., Khvat, A., Schnabl, B., Yu,
742 R. T., Brenner, D. A., Coulter, S., Liddle, C., Schoonjans, K., Olefsky, J. M., . . .
743 Evans, R. M. (2015). Intestinal FXR agonism promotes adipose tissue browning
744 and reduces obesity and insulin resistance. *Nat Med*, *21*(2), 159-165.
745 https://doi.org/10.1038/nm.3760
746 Friedman, S. L., Neuschwander-Tetri, B. A., Rinella, M., & Sanyal, A. J. (2018).
747 Mechanisms of NAFLD development and therapeutic strategies. *Nat Med*, *24*(7),
748 908-922. https://doi.org/10.1038/s41591-018-0104-9
749 Gerstberger, S., Hafner, M., & Tuschl, T. (2014). A census of human RNA-binding
750 proteins. *Nat Rev Genet*, *15*(12), 829-845. https://doi.org/10.1038/nrg3813
751 Giudice, G., Sanchez-Cabo, F., Torroja, C., & Lara-Pezzi, E. (2016). ATtRACT-a
752 database of RNA-binding proteins and associated motifs. *Database (Oxford)*,
753 *2016*. https://doi.org/10.1093/database/baw035
754 Goodwin, B., Jones, S. A., Price, R. R., Watson, M. A., McKee, D. D., Moore, L. B.,
755 Galardi, C., Wilson, J. G., Lewis, M. C., Roth, M. E., Maloney, P. R., Willson, T.
756 M., & Kliewer, S. A. (2000). A regulatory cascade of the nuclear receptors FXR,
757 SHP-1, and LRH-1 represses bile acid biosynthesis. *Mol Cell*, *6*(3), 517-526.
758 https://doi.org/10.1016/s1097-2765(00)00051-4
759 Heinz, S., Benner, C., Spann, N., Bertolino, E., Lin, Y. C., Laslo, P., Cheng, J. X.,
760 Murre, C., Singh, H., & Glass, C. K. (2010). Simple combinations of lineage-
761 determining transcription factors prime cis-regulatory elements required for
762 macrophage and B cell identities. *Mol Cell*, *38*(4), 576-589.
763 https://doi.org/10.1016/j.molcel.2010.05.004
764 Hernandez, E. D., Zheng, L., Kim, Y., Fang, B., Liu, B., Valdez, R. A., Dietrich, W. F.,
765 Rucker, P. V., Chianelli, D., Schmeits, J., Bao, D., Zoll, J., Dubois, C., Federe, G.
766 C., Chen, L., Joseph, S. B., Klickstein, L. B., Walker, J., Molteni, V., . . . Laffitte,
767 B. (2019). Tropifexor-Mediated Abrogation of Steatohepatitis and Fibrosis Is
768 Associated With the Antioxidative Gene Expression Profile in Rodents. *Hepatol*
769 *Commun*, *3*(8), 1085-1097. https://doi.org/10.1002/hep4.1368
770 Hirabayashi, S., Bhagat, S., Matsuki, Y., Takegami, Y., Uehata, T., Kanemaru, A., Itoh,
771 M., Shirakawa, K., Takaori-Kondo, A., Takeuchi, O., Carninci, P., Katayama, S.,
772 Hayashizaki, Y., Kere, J., Kawaji, H., & Murakawa, Y. (2019). NET-CAGE
773 characterizes the dynamics and topology of human transcribed cis-regulatory

774 elements. *Nat Genet*, *51*(9), 1369-1379. https://doi.org/10.1038/s41588-019-
775 0485-9
776 Hon, C. C., Ramilowski, J. A., Harshbarger, J., Bertin, N., Rackham, O. J., Gough, J.,
777 Denisenko, E., Schmeier, S., Poulsen, T. M., Severin, J., Lizio, M., Kawaji, H.,
778 Kasukawa, T., Itoh, M., Burroughs, A. M., Noma, S., Djebali, S., Alam, T.,
779 Medvedeva, Y. A., . . . Forrest, A. R. (2017). An atlas of human long non-coding
780 RNAs with accurate 5' ends. *Nature*, *543*(7644), 199-204.
781 https://doi.org/10.1038/nature21374
782 Hsieh, C. L., Fei, T., Chen, Y., Li, T., Gao, Y., Wang, X., Sun, T., Sweeney, C. J., Lee,
783 G. S., Chen, S., Balk, S. P., Liu, X. S., Brown, M., & Kantoff, P. W. (2014).
784 Enhancer RNAs participate in androgen receptor-driven looping that selectively
785 enhances gene activation. *Proc Natl Acad Sci U S A*, *111*(20), 7319-7324.
786 https://doi.org/10.1073/pnas.1324151111
787 Jung, H., Chen, J., Hu, X., Sun, H., Wu, S. Y., Chiang, C. M., Kemper, B., Chen, L. F., &
788 Kemper, J. K. (2020). BRD4 inhibition and FXR activation, individually beneficial
789 in cholestasis, are antagonistic in combination. *JCI Insight*, *6*(1).
790 https://doi.org/10.1172/jci.insight.141640
791 Kim, D. H., Kwon, S., Byun, S., Xiao, Z., Park, S., Wu, S. Y., Chiang, C. M., Kemper, B.,
792 & Kemper, J. K. (2016). Critical role of RanBP2-mediated SUMOylation of Small
793 Heterodimer Partner in maintaining bile acid homeostasis. *Nat Commun*, *7*,
794 12179. https://doi.org/10.1038/ncomms12179
795 Kim, Y. C., Fang, S., Byun, S., Seok, S., Kemper, B., & Kemper, J. K. (2015). Farnesoid
796 X receptor-induced lysine-specific histone demethylase reduces hepatic bile acid
797 levels and protects the liver against bile acid toxicity. *Hepatology*, *62*(1), 220-231.
798 https://doi.org/10.1002/hep.27677
799 Kim, Y. C., Jung, H., Seok, S., Zhang, Y., Ma, J., Li, T., Kemper, B., & Kemper, J. K.
800 (2020). MicroRNA-210 Promotes Bile Acid-Induced Cholestatic Liver Injury by
801 Targeting Mixed-Lineage Leukemia-4 Methyltransferase in Mice. *Hepatology*,
802 *71*(6), 2118-2134. https://doi.org/10.1002/hep.30966
803 Kleene, K. C. (2018). Y-box proteins combine versatile cold shock domains and
804 arginine-rich motifs (ARMs) for pleiotropic functions in RNA biology. *Biochem J*,
805 *475*(17), 2769-2784. https://doi.org/10.1042/BCJ20170956
806 Kliewer, S. A., & Mangelsdorf, D. J. (2015). Bile Acids as Hormones: The FXR-
807 FGF15/19 Pathway. *Dig Dis*, *33*(3), 327-331. https://doi.org/10.1159/000371670
808 Kremoser, C. (2021). FXR agonists for NASH: How are they different and what
809 difference do they make? *J Hepatol*, *75*(1), 12-15.
810 https://doi.org/10.1016/j.jhep.2021.03.020
811 Lai, F., & Shiekhattar, R. (2014). Enhancer RNAs: the new molecules of transcription.
812 *Curr Opin Genet Dev*, *25*, 38-42. https://doi.org/10.1016/j.gde.2013.11.017
813 Lam, M. T., Li, W., Rosenfeld, M. G., & Glass, C. K. (2014). Enhancer RNAs and
814 regulated transcriptional programs. *Trends Biochem Sci*, *39*(4), 170-182.
815 https://doi.org/10.1016/j.tibs.2014.02.007
816 Lee, F. Y., Lee, H., Hubbert, M. L., Edwards, P. A., & Zhang, Y. (2006). FXR, a
817 multipurpose nuclear receptor. *Trends Biochem Sci*, *31*(10), 572-580.
818 https://doi.org/10.1016/j.tibs.2006.08.002
819 Lee, J., Padhye, A., Sharma, A., Song, G., Miao, J., Mo, Y. Y., Wang, L., & Kemper, J.

K. (2010). A pathway involving farnesoid X receptor and small heterodimer partner positively regulates hepatic sirtuin 1 levels via microRNA-34a inhibition. *J Biol Chem*, *285*(17), 12604-12611. https://doi.org/10.1074/jbc.M109.094524

Lee, J., Seok, S., Yu, P., Kim, K., Smith, Z., Rivas-Astroza, M., Zhong, S., & Kemper, J. K. (2012). Genomic analysis of hepatic farnesoid X receptor binding sites reveals altered binding in obesity and direct gene repression by farnesoid X receptor in mice. *Hepatology*, *56*(1), 108-117. https://doi.org/10.1002/hep.25609

Lee, J. M., Wagner, M., Xiao, R., Kim, K. H., Feng, D., Lazar, M. A., & Moore, D. D. (2014). Nutrient-sensing nuclear receptors coordinate autophagy. *Nature*, *516*(7529), 112-115. https://doi.org/10.1038/nature13961

Li, J., Woolbright, B. L., Zhao, W., Wang, Y., Matye, D., Hagenbuch, B., Jaeschke, H., & Li, T. (2018). Sortilin 1 Loss-of-Function Protects Against Cholestatic Liver Injury by Attenuating Hepatic Bile Acid Accumulation in Bile Duct Ligated Mice. *Toxicol Sci*, *161*(1), 34-47. https://doi.org/10.1093/toxsci/kfx078

Li, W., Notani, D., Ma, Q., Tanasa, B., Nunez, E., Chen, A. Y., Merkurjev, D., Zhang, J., Ohgi, K., Song, X., Oh, S., Kim, H. S., Glass, C. K., & Rosenfeld, M. G. (2013). Functional roles of enhancer RNAs for oestrogen-dependent transcriptional activation. *Nature*, *498*(7455), 516-520. https://doi.org/10.1038/nature12210

Li, W., Notani, D., & Rosenfeld, M. G. (2016). Enhancers as non-coding RNA transcription units: recent insights and future perspectives. *Nat Rev Genet*, *17*(4), 207-223. https://doi.org/10.1038/nrg.2016.4

Li, Y., Tan, Z., Zhang, Y., Zhang, Z., Hu, Q., Liang, K., Jun, Y., Ye, Y., Li, Y. C., Li, C., Liao, L., Xu, J., Xing, Z., Pan, Y., Chatterjee, S. S., Nguyen, T. K., Hsiao, H., Egranov, S. D., Putluri, N., . . . Yang, L. (2021). A noncoding RNA modulator potentiates phenylalanine metabolism in mice. *Science*, *373*(6555), 662-673. https://doi.org/10.1126/science.aba4991

Love, M. I., Huber, W., & Anders, S. (2014). Moderated estimation of fold change and dispersion for RNA-seq data with DESeq2. *Genome Biol*, *15*(12), 550. https://doi.org/10.1186/s13059-014-0550-8

Mattick, J. S., Amaral, P. P., Carninci, P., Carpenter, S., Chang, H. Y., Chen, L. L., Chen, R., Dean, C., Dinger, M. E., Fitzgerald, K. A., Gingeras, T. R., Guttman, M., Hirose, T., Huarte, M., Johnson, R., Kanduri, C., Kapranov, P., Lawrence, J. B., Lee, J. T., . . . Wu, M. (2023). Long non-coding RNAs: definitions, functions, challenges and recommendations. *Nat Rev Mol Cell Biol*, *24*(6), 430-447. https://doi.org/10.1038/s41580-022-00566-8

Mirtschink, P., Bischof, C., Pham, M. D., Sharma, R., Khadayate, S., Rossi, G., Fankhauser, N., Traub, S., Sossalla, S., Hagag, E., Berthonneche, C., Sarre, A., Stehr, S. N., Grote, P., Pedrazzini, T., Dimmeler, S., Krek, W., & Krishnan, J. (2019). Inhibition of the Hypoxia-Inducible Factor 1alpha-Induced Cardiospecific HERNA1 Enhance-Templated RNA Protects From Heart Disease. *Circulation*, *139*(24), 2778-2792. https://doi.org/10.1161/CIRCULATIONAHA.118.036769

Oh, S., Shao, J., Mitra, J., Xiong, F., D'Antonio, M., Wang, R., Garcia-Bassets, I., Ma, Q., Zhu, X., Lee, J. H., Nair, S. J., Yang, F., Ohgi, K., Frazer, K. A., Zhang, Z. D., Li, W., & Rosenfeld, M. G. (2021). Enhancer release and retargeting activates disease-susceptibility genes. *Nature*, *595*(7869), 735-740. https://doi.org/10.1038/s41586-021-03577-1

Rahnamoun, H., Lee, J., Sun, Z., Lu, H., Ramsey, K. M., Komives, E. A., & Lauberth, S. M. (2018). RNAs interact with BRD4 to promote enhanced chromatin engagement and transcription activation. *Nat Struct Mol Biol*, *25*(8), 687-697. https://doi.org/10.1038/s41594-018-0102-0

Sallam, T., Jones, M. C., Gilliland, T., Zhang, L., Wu, X., Eskin, A., Sandhu, J., Casero, D., Vallim, T. Q., Hong, C., Katz, M., Lee, R., Whitelegge, J., & Tontonoz, P. (2016). Feedback modulation of cholesterol metabolism by the lipid-responsive non-coding RNA LeXis. *Nature*, *534*(7605), 124-128. https://doi.org/10.1038/nature17674

Sanyal, A. J., Lopez, P., Lawitz, E. J., Lucas, K. J., Loeffler, J., Kim, W., Goh, G. B. B., Huang, J. F., Serra, C., Andreone, P., Chen, Y. C., Hsia, S. H., Ratziu, V., Aizenberg, D., Tobita, H., Sheikh, A. M., Vierling, J. M., Kim, Y. J., Hyogo, H., . . . Brass, C. A. (2023). Tropifexor for nonalcoholic steatohepatitis: an adaptive, randomized, placebo-controlled phase 2a/b trial. *Nat Med*, *29*(2), 392-400. https://doi.org/10.1038/s41591-022-02200-8

Sartorelli, V., & Lauberth, S. M. (2020). Enhancer RNAs are an important regulatory layer of the epigenome. *Nat Struct Mol Biol*, *27*(6), 521-528. https://doi.org/10.1038/s41594-020-0446-0

Seok, S., Fu, T., Choi, S. E., Li, Y., Zhu, R., Kumar, S., Sun, X., Yoon, G., Kang, Y., Zhong, W., Ma, J., Kemper, B., & Kemper, J. K. (2014). Transcriptional regulation of autophagy by an FXR-CREB axis. *Nature*, *516*(7529), 108-111. https://doi.org/10.1038/nature13949

Seok, S., Kim, Y. C., Byun, S., Choi, S., Xiao, Z., Iwamori, N., Zhang, Y., Wang, C., Ma, J., Ge, K., Kemper, B., & Kemper, J. K. (2018). Fasting-induced JMJD3 histone demethylase epigenetically activates mitochondrial fatty acid beta-oxidation. *J Clin Invest*, *128*(7), 3144-3159. https://doi.org/10.1172/JCI97736

Seok, S., Sun, H., Kim, Y. C., Kemper, B., & Kemper, J. K. (2021). Defective FXR-SHP Regulation in Obesity Aberrantly Increases miR-802 Expression, Promoting Insulin Resistance and Fatty Liver. *Diabetes*, *70*(3), 733-744. https://doi.org/10.2337/db20-0856

Statello, L., Guo, C. J., Chen, L. L., & Huarte, M. (2021). Gene regulation by long non-coding RNAs and its biological functions. *Nat Rev Mol Cell Biol*, *22*(2), 96-118. https://doi.org/10.1038/s41580-020-00315-9

Sun, H., Seok, S., Jung, H., Kemper, B., & Kemper, J. K. (2022). Obesity-induced miR-802 directly targets AMPK and promotes nonalcoholic steatohepatitis in mice. *Mol Metab*, *66*, 101603. https://doi.org/10.1016/j.molmet.2022.101603

Tang, X., Luo, Y., Yuan, D., Calandrelli, R., Malhi, N. K., Sriram, K., Miao, Y., Lou, C. H., Tsark, W., Tapia, A., Chen, A. T., Zhang, G., Roeth, D., Kalkum, M., Wang, Z. V., Chien, S., Natarajan, R., Cooke, J. P., Zhong, S., & Chen, Z. B. (2023). Long noncoding RNA LEENE promotes angiogenesis and ischemic recovery in diabetes models. *J Clin Invest*, *133*(3). https://doi.org/10.1172/JCI161759

Thomas, A. M., Hart, S. N., Kong, B., Fang, J., Zhong, X. B., & Guo, G. L. (2010). Genome-wide tissue-specific farnesoid X receptor binding in mouse liver and intestine. *Hepatology*, *51*(4), 1410-1419. https://doi.org/10.1002/hep.23450

Tully, D. C., Rucker, P. V., Chianelli, D., Williams, J., Vidal, A., Alper, P. B., Mutnick, D., Bursulaya, B., Schmeits, J., Wu, X., Bao, D., Zoll, J., Kim, Y., Groessl, T.,

McNamara, P., Seidel, H. M., Molteni, V., Liu, B., Phimister, A., . . . Laffitte, B. (2017). Discovery of Tropifexor (LJN452), a Highly Potent Non-bile Acid FXR Agonist for the Treatment of Cholestatic Liver Diseases and Nonalcoholic Steatohepatitis (NASH). *J Med Chem*, *60*(24), 9960-9973. https://doi.org/10.1021/acs.jmedchem.7b00907

Wahlstrom, A., Sayin, S. I., Marschall, H. U., & Backhed, F. (2016). Intestinal Crosstalk between Bile Acids and Microbiota and Its Impact on Host Metabolism. *Cell Metab*, *24*(1), 41-50. https://doi.org/10.1016/j.cmet.2016.05.005

Wang, Y. D., Chen, W. D., Wang, M., Yu, D., Forman, B. M., & Huang, W. (2008). Farnesoid X receptor antagonizes nuclear factor kappaB in hepatic inflammatory response. *Hepatology*, *48*(5), 1632-1643. https://doi.org/10.1002/hep.22519

Warren, C. F. A., Wong-Brown, M. W., & Bowden, N. A. (2019). BCL-2 family isoforms in apoptosis and cancer. *Cell Death Dis*, *10*(3), 177. https://doi.org/10.1038/s41419-019-1407-6

Zhao, X. Y., Xiong, X., Liu, T., Mi, L., Peng, X., Rui, C., Guo, L., Li, S., Li, X., & Lin, J. D. (2018). Long noncoding RNA licensing of obesity-linked hepatic lipogenesis and NAFLD pathogenesis. *Nat Commun*, *9*(1), 2986. https://doi.org/10.1038/s41467-018-05383-2

Zheng, W., Lu, Y., Tian, S., Ma, F., Wei, Y., Xu, S., & Li, Y. (2018). Structural insights into the heterodimeric complex of the nuclear receptors FXR and RXR. *J Biol Chem*, *293*(32), 12535-12541. https://doi.org/10.1074/jbc.RA118.004188

Zou, C., Wan, Y., He, L., Zheng, J. H., Mei, Y., Shi, J., Zhang, M., Dong, Z., & Zhang, D. (2021). RBM38 in cancer: role and mechanism. *Cell Mol Life Sci*, *78*(1), 117-128. https://doi.org/10.1007/s00018-020-03593-w

958 **Figure legends**

959 **Figure 1. Activation of FXR by GW4064 induces *FincoR*, a novel eRNA, in mouse**
960 **liver.** (A) Volcano plot from RNA-Seq showing significantly induced eRNAs (*FincoR* is
961 highlighed) in the livers of C57BL/6 male mice treated with GW4064 (*i.p*. injection, 30
962 mg/kg, 1 h) or vehicle. The *x* axis denotes $\log_2$ fold change (GW4064/Veh) of eRNAs and
963 the *y* axis denotes $-\log_{10}$ FDR of eRNAs. (B) A Bar plot showing the reads per million
964 (RPMs) of up regulated eRNAs by GW4064 treatment. (C) IGV genome browser track
965 showing RNA-seq signals from vehicle or GW4064 treated samples around the *FincoR*
966 locus and its neighboring regions. A zoom-in view of *FincoR* is shown below. Veh, vehicle;
967 GW, GW4064; pos, positive strand; neg, negative strand; Refseq, reference sequence.
968 (D) RT-qPCR data showing GW4064 induction of *FincoR* eRNA and *Shp* mRNA in the
969 liver (n=4/group). Data are presented as mean ± SEM. Statistical significance was
970 determined by the two-way ANOVA Sidak's multiple comparisons test with $^{**}p < 0.01$ and
971 $^{***}p < 0.001$.

972 **Figure 2. Ligand-activated FXR directly activates transcription of eRNAs including**
973 ***FincoR* in the liver.** (A) Left: experimental outline. FXR-Flox and LKO male mice were
974 fasted overnight and treated with vehicle or GW4064, and livers were collected 1 h later
975 with nuclei isolated for Gro-seq (n=2/group). Right: a boxplot shows the Gro-Seq signals
976 for GW4064 up-regulated eRNAs in different conditions. RPKM: reads per kbp per million.
977 (B) IGV genome browser track showing RNA-seq, Gro-seq and ChIP-seq signals in the
978 *FincoR* locus. An arrow at the bottom points to the main enhancer FXR ChIP-seq peak
979 that overlaps the start site of *FincoR*. (C) ChIP assays were performed in the same liver
980 samples described in Fig. 1A to detect FXR, RXRα, and BRD4 occupancy at the FXR

981 binding peak region close to the transcription start site of *FincoR* (black arrow in Fig.2B).
982 (D) HepG2 cells were transfected with luciferase reporter expressing wild type FXRE or
983 mutant FXRE (see materials and methods) for 24 h before treatment with GW4064 for an
984 additional 6 h. Relative luciferase activities are shown. (C-D) Data are presented as
985 mean ± SEM. Statistical significance was determined by the Student's t test with *$p < 0.05$
986 and ***$p < 0.001$.
987

988 **Figure 3. *FincoR* is a liver-specific nucleus-enriched eRNA.** (A) Expression levels of
989 *FincoR* in various tissues after GW4064 treatment. Data from C57BL/6 male mice fasted
990 overnight and *i.p.* injected with vehicle or GW4064 (30 mg/kg) for 1 h (n=2/group). (B)
991 C57BL/6 male mice were fasted overnight and injected *i.p.* with vehicle or GW4064 (30
992 mg/kg) for 1 h. One small piece of liver was snap-frozen for later RNA isolation and the
993 remaining part was used for immediate primary hepatocyte isolation. Then, RNAs were
994 extracted from liver or primary hepatocytes and *FincoR* expression was measured
995 (n=3/group). (C) Agarose gel electrophoresis of PCR products generated in 5′ (left) and
996 3′ (right) RACE of *FincoR* in liver samples. Primer locations are shown. RACE, rapid
997 amplification of cDNA ends. GSP: gene specific primer. (D) A schematic diagram
998 showing location of *FincoR* relative to nearby genes in the mice genome. (E) PhyloCSF
999 analysis of the coding potential of *FincoR*. (F) In vitro translation of *FincoR* using the
1000 Promega Transcend Non-Radioactive Translation Detection Systems. Luciferase is used
1001 as a control for coding RNA. (G) qPCR analysis of *FincoR*, *36b4* in Poly(A)+ and Poly(A)-
1002 RNA fractions from GW4064 treated mouse liver. (H) *FincoR* identified in the subcellular
1003 fractions using cellular fractionation assays. Primary hepatocytes were isolated from

1004 GW4064 or DMSO treated mice and the cytoplasm and nucleus fractions of these
1005 hepatocytes were separated and both fractions were subjected to RNA extraction and
1006 qPCR.

1007 **Figure 4. *FincoR* is induced by the hammerhead class of non-steroidal FXR**
1008 **agonists, including GW4064 and tropifexor.** (A) The chemical structures of the FXR
1009 agonists including the hammerhead class of synthetic FXR agonists, non-hammerhead-
1010 type synthetic agonists, semi-synthetic BA and natural BA. BA: bile acid. (B) qPCR data
1011 showing *FincoR* expression levels in C57BL/6 mice liver respectively treated with
1012 GW4064 (30 mg/kg), Cilofexor (30 mg/kg), Tropifexor (0.5 mg/kg), Fexaramine (100
1013 mg/kg), or OCA (20 mg/kg) for 1 h (n=3~4/group). (C) *FincoR* expression levels in
1014 C57BL/6 mice liver treated with OCA (20 mg/kg) or Fexaramine (100 mg/kg) for 4 hrs
1015 (n=3/group). (D) Expression of *FincoR* in C57BL/6 mice liver after daily treatment with
1016 OCA (20 mg/kg) for 7 days (n=5/group). *Shp* gene mRNA was measured as a positive
1017 control. (E) Expression of *FincoR* in C57BL/6 mice fed with 0.5% cholic acid (CA) diet for
1018 6 hrs (n=3~4/group). In panels B-E, all mice underwent over-night fasting. (B-E) Data are
1019 presented as mean ± SEM. Statistical significance was determined by the Student's t test
1020 with $*p < 0.05$, $**p < 0.01$ and $***p < 0.001$.

1021 **Figure 5. Generation of CRISPR/Cas9-mediated *FincoR* liver-specific knockdown**
1022 **mice.** (A) Experimental scheme: male Cas9 mice were infected with adenovirus
1023 expressing sgRNA for *FincoR* or a control for 1 week. Then the liver and serum were
1024 collected from these mice after 4~5 hrs of fasting. (B) The expression of *FincoR* in the
1025 liver was measured by qPCR (n=4/group). (C) Hepatic triglyceride, cholesterol, bile acid,
1026 glycogen and serum NEFA were measured (n=5~7/group) (D) Male Cas9 mice were

1027 infected with adenovirus expressing sgRNA for *FincoR* or control for 1 week. Then these
1028 mice were fasted overnight and treated with GW4064 for 3 h before tissue collection.
1029 RNA-seq profiles of expression of hepatic *FincoR* and the adjacent genes were shown
1030 (n=2/group). (E) Genome-wide changes in mRNA expression shown in a volcano plot.
1031 The numbers refer to the number of genes up- or down-regulated by 2-fold or more with
1032 an adjusted *p*-value < 0.01. (F) Gene ontology analysis of biological pathways using
1033 DAVID Tools for genes downregulated after *FincoR* knockdown. (B) Data are presented
1034 as mean ± SEM. Statistical significance was determined by the Student's t test with ***p <
1035 0.001.

1036 **Figure 6. In diet-induced NASH mice, tropifexor-mediated beneficial effects on**
1037 **reducing hepatic steatosis are largely independent of *FincoR*.** (A-E) Male Cas9 mice
1038 were fed a NASH diet for 12 weeks. The mice were randomly assigned to 3 groups and
1039 infected with adenovirus expressing sgRNA for *FincoR* or control. Three days later, the
1040 mice were treated with tropifexor (0.3 mg/kg) or vehicle for 12 days. The mice were
1041 administered tropifexor or vehicle and fasted for 4 h before tissues were collected. (A)
1042 Experimental scheme. (B) Hepatic *FincoR* expression was measured (n=6~7/group). (C)
1043 Oil Red O staining of liver sections. Scale bar (50 μm). Image analyses were done using
1044 Image J and the areas of stained field were quantified (n=5/group) (D) Hepatic TG,
1045 hepatic cholesterol, gallbladder BA and hepatic BA levels were measured (n=6~7/group).
1046 (E) mRNA levels in the liver of the indicated genes involved in bile acid regulation and
1047 lipid regulation (n=6~7/group). (B, D and E) Data are presented as mean ± SEM.
1048 Statistical significance was determined by the one-way ANOVA (Sidak's multiple

1049 comparisons test) with *$p < 0.05$, **$p < 0.01$ and ***$p < 0.001$. Ad, adenovirus; H & E,
1050 hematoxylin and eosin; TG, triglyceride; Veh, vehicle; ns, not significant.

1051 **Figure 7. In diet-induced NASH mice, tropifexor-mediated beneficial effects on**
1052 **reducing liver fibrosis and inflammation are diminished by *FincoR* downregulation.**
1053 (A) Representative images from H & E, F4/80, Sirius Red and TUNEL staining of liver
1054 sections from the same cohort of mice described in Figure 6. Scale bar (50 μm). Image
1055 analyses were done using Image J and the area of collagen staining, TUNEL and F4/80
1056 levels were quantified (n=5/group). (B) Serum ALT and AST levels were measured
1057 (n=5/group). (C) IL-1β and CCL2 levels in the liver tissues were determined by ELISA
1058 (n=5/group). (D) mRNA levels in the liver of the indicated genes involved in inflammation,
1059 fibrosis and cell death (n=5/group). (E) Model: *FincoR* is a liver-enriched eRNA that is
1060 induced specifically by hammerhead-type FXR agonists (top). In diet-induced NASH
1061 mice, *FincoR* is required for tropifexor-mediated beneficial effects on reducing hepatic
1062 inflammation, fibrosis, and cell death with the mechanisms to be determined (bottom). (A-
1063 D) Data are presented as mean ± SEM. Statistical significance was determined by the
1064 one-way ANOVA (Sidak's multiple comparisons test) with *$p < 0.05$, **$p < 0.01$ and ***$p <$
1065 0.001.

1066

1067

1068 **Supplementary Figure Legends**

1069 **Figure 1- figure supplement 1.** (A, B) Examples of FXR-regulated eRNAs produced
1070 near the genes *Hes1* (A) and *Slc35g1* (B) were shown. (C) Time course expression of
1071 *FincoR*. C57BL/6 male mice were fasted overnight and injected *i.p.* with vehicle or
1072 GW4064 (30 mg/kg) for 1, 3, 6,12 h. Livers were collected at the indicated time points
1073 (n=3/group) and *FincoR* and mRNA levels of *Shp* and *Gcnt1* were measured. Data are
1074 presented as mean ± SEM. Statistical significance was determined by the two-way
1075 ANOVA Sidak's multiple comparisons test with $*p < 0.05$ and $***p < 0.001$.

1076 **Figure 1- figure supplement 2.** (A) Volcano plot showing the differential expressed
1077 genes (DEGs) after GW4064 treatment (DESeq2 FDR<0.05). The numbers refer to the
1078 number of genes up- or down-regulated. (B) Bar plot showing the enriched Gene
1079 Ontology in terms of biological processes for up-regulated genes.

1080 **Figure 2- figure supplement 1**. (A) FXR protein levels in the livers isolated from FXR-
1081 Flox and FXR-LKO mice are shown. (B) Validation of hepatic FXR-dependent induction
1082 of *FincoR* by qPCR (n = 3 mice). The *Shp* gene was used as a control. Data are presented
1083 as mean ± SEM. Statistical significance was determined by the two-way ANOVA Tukey's
1084 multiple comparisons test with $*p < 0.05$ and $**p < 0.01$. (C) Metagene plots showing
1085 H3K27ac, H3K4me1, FXR, and RXRα ChIP-Seq profiles centered on up-regulated
1086 eRNAs.

1087 **Figure 5- figure supplement 1**. (A) Left: experimental scheme for the *FincoR* loss of
1088 function experiments. Right: illustration demonstrating the sequence targeted by the
1089 sgRNA in relation to the transcriptional and epigenetic profile. (B) The genomic DNAs
1090 from liver, spleen, intestine, brain, heart, muscle, kidney, lung and adipose tissue were

1091 isolated and PCR was performed using the primers (**Supplementary Table S6**) to verify
1092 tissue-specific knock-out. (C-G) RNA-seq profiles of expression of hepatic *Prune2* (C),
1093 *PPP1r3g* (D), *Igfbp2* (E), *Eda2r* (F) *and Fndc1* (G) are shown (n=2/group).
1094 **Figure 7- figure supplement 1. The effects of *FincoR* downregulation on NASH**
1095 **pathologies.** Male Cas9 mice were fed with a NASH diet for 12 weeks. Then these mice
1096 were randomly assigned to 2 groups and infected with adenovirus expressing sgRNA for
1097 *FincoR* or control. The tissues were collected 2 weeks later. Liver histology analysis was
1098 performed and representative images were shown. Scale bar (50 μm).
1099
1100 **Supplementary Figure S1. Hepatic expression of *FincoR* is elevated in liver disease**
1101 **associated with inflammation and fibrosis.** (A) C57BL/6 mice were fed with a high fat
1102 diet for 12 weeks. The liver RNAs were extracted and *FincoR* expression was measured
1103 (n=5/group). (B) C57BL/6 mice were fed with a high fat diet with high fructose water for
1104 12 weeks. The liver RNAs were extracted and *FincoR* expression was measured
1105 (n=7/group). (C) C57BL/6 mice were treated with ANIT (75 mg/kg) for 48 h and then
1106 sacrificed after 5 h of fasting. The liver RNAs were extracted, and *FincoR* expression was
1107 measured (n=4~5/group). (D) C57BL/6 mice were bile duct ligated for 1 day or 3 days.
1108 They were then sacrificed after 5 h of fasting. The liver RNAs were extracted and *FincoR*
1109 expression was measured (n=4~5/group). (E) *FincoR* conservation between mice and
1110 human as displayed in the UCSC Genome Browser. Red arrows indicate the conserved
1111 region. (F) Human lncRNA XR_007061585.1 with sequence similarity to mouse *FincoR*
1112 annotated in the NCBI genome data viewer. (G) Expression of lncRNA XR_007061585.1
1113 in liver samples from normal individuals or patients with primary biliary cholangitis (PBC)

1114 (n=14~15/group). (H) Expression of lncRNA XR_007061585.1 in liver samples from
1115 normal individuals or patients with NAFLD-associated steatosis (n=12~15/group). (A-D,
1116 G-H) Data are presented as mean ± SEM. Statistical significance was determined by the
1117 Student's t test with *$p < 0.05$, **$p < 0.01$ and ***$p < 0.001$.

1118 **Supplementary Figure S2. Hepatic genome browser tracks of FXR, RXRα, LXR,**
1119 **PPARα, and HNF4α binding peaks at the *FincoR* locus.**

1120 **Supplementary Figure S3. PPARα occupancy in the *FincoR* enhancer region.**
1121 C57BL/6 male mice were fasted overnight with or without refeeding for 3 h and then
1122 sacrificed. ChIP assays were performed in liver samples to detect PPARα occupancy at
1123 the FXR binding peak region close to the transcription start site of *FincoR*.

1124

1125

1126

1127
1128
1129
1130
1131

1132 **Supplemental Tables**

1133

1134 Supplemental Table S1. Sequencing data generated in this study

Name	Total reads	Uniquely mapped reads
WT Liver Veh RNA-Seq rep1	50887391	38072659
WT Liver GW RNA-Seq rep1	54020150	40595856
WT Liver Veh RNA-Seq rep2	51268164	38898913
WT Liver GW RNA-Seq rep2	51899892	39487241
Flox Liver Veh GRO-Seq	62960996	30305910
Flox Liver GW GRO-Seq	59210073	26116795
FXR KO Liver Veh GRO-Seq	34153537	14379417
FXR KO Liver GW GRO-Seq	36430101	15008281
WT Liver RNA-Seq rep1	96262381	81801494
WT Liver RNA-Seq rep2	104979915	88365481
FincoR KD Liver RNA-Seq rep1	91654076	75346167
FincoR KD Liver RNA-Seq rep2	90211420	74745807

1135

1136 Supplemental Table S2 is attached as an Excel file.

1137

1138 Supplemental Table S3. Public ChIP-Seq dataset

target	accession ID
FXR	https://genome.ucsc.edu/cgi-bin/hgCustom?hgsid=1577671033_RPWVA7jbx3rDswKOeo2dazTsXxe0&hgct_table=ct_FxrLiver_2971
H3K27ac	ENCFF001KMI
H3K4me1	ENCFF001KNF
LXR	GSM864669
RXRα	GSM864674
PPARα	GSM864671
HNF4α	GSM2055887

1139

1140 Supplemental Table S4 is attached as an Excel file.

1141

1142 Supplemental Table S5: Predicted RNA binding proteins (RBPs) binding to *FincoR*

RBP	Length	Motif	Domain	number of binding sites
KHDRBS1	7	UAAAAAG	KH	1
RBM38	7	UUGUGUG, GUGUGUG	RRM	3
YBX2	7	CACACCA	CSD	11
YBX3	7	CACACCA	CSD	11
PCBP1	6	CUUUCC	KH	1
KHSRP	6	UGCAUG	KH	2
PTBP1	6	CUCUCU	RRM	1
PTBP2	6	CUCUCU	RRM	1
4KZD	5	GAAAC	N/A	1
4KZE	5	GAAAC	N/A	1
4Q9Q	5	GAAAC	N/A	1
DAZL	5	GUUCU	RRM	6

MSI1	5	GUAGU	RRM	1
TLR3	5	AAAGG	LRR;TIR	12

1143
1144
1145 Supplemental Table S6. Primer sequences used in this study
1146
1147 A. List of primer sequences for mouse qRT-PCR

Gene	Forward Primer (5'-3')	Reverse Primer (5'-3')
FincoR	GCAAAGCACCTTCTAGCACA	GTCAGGGAGCTAACGAATGC
Gcnt1	GCATCGCATCCTGCTTTGATA	GGTCTGCCTTAACCCGACTC
Shp	TCTGCAGGTCGTCCGACTAT	CAGGCAGTGGCTGTGAGAT
Cyp7a1	GGGATTGCTGTGGTAGTGAGC	GGTATGGAATCAACCCGTTGTC
Cyp8b1	CCTCTGGACAAGGGTTTTGTG	GCACCGTGAAGACATCCCC
Srebp1c	GCAGCCACCATCTAGCCTG	CAGCAGTGAGTCTGCCTTGAT
Lpin1	CATGCTTCGGAAAGTCCTTCA	GGTTATTCTTTGGCGTCAACCT
Scd1	TTCTTGCGATACACTCTGGTGC	CGGGATTGAATGTTCTTGTCGT
Ifng	GCG TCA TTG AAT CAC ACC TG	GAC CTG TGG GTT GTT GAC CT
Ccl3	TTCTCTGTACCATGACACTCTGC	CGTGGAATCTTCCGGCTGTAG
Ccl2	TTAAAAACCTGGATCGGAACCAA	GCATTAGCTTCAGATTTACGGGT
Ccr2	AAGAGGGCATTGGATTCACCACA	GCCGTGGATGAACTGAGGTAACA
Lcn2	GCAGGTGGTACGTTGTGGG	CTCTTGTAGCTCATAGATGGTGC
Col1a1	ATCGGTCATGCTCTCTCCAAACCA	ACTGCAACATGGAGACAGGTCAGA
Col1a2	CCTTTGTCAGAATACTGAGCAGC	GTAACTTCGTGCCTAGCAACA
Acta2	TCGGATACTTCAGCGTCAGGA	GTCCCAGACATCAGGGAGTAA
Eda2r	CACACTGCATAGTCTGCCCTC	GCCTTCTGGACCCGATTGA
Fndc1	GGGAGACATGGCAAACCTGT	TGGTAGGAGAGTATGTGGTGG
Ctsb	TCCTTGATCCTTCTTTCTTGCC	ACAGTGCCACACAGCTTCTTC
Ctss	GAAGTACGGCGTCTCATCTGG	CATGCCCACTTGGTAGGTATG
Bcl2	GTCGCTACCGTCGTGACTTC	CAGACATGCACCTACCCAGC
36b4	CCCTGAAGTGCTCGACATCA	TGCGGACACCCTCCAGAA
XR_007061585.1	TTGTCATCAAGCCCTGTTCA	TCTGCTTTGTCTGAGGACCA

1148
1149 B. List of primers used for mutagenesis

	Forward Primer (5'-3')	Reverse Primer (5'-3')
Mutation	GTGAATTCTCTCCTAGaTCcTTGACaTTCCAAGTC ATGTAC	GTACATGACTTGGAAtGTCAAgGAtCTAGGAGAGAATTC AC

1150
1151

1152 C. List of primer sequences for mouse ChIP-qPCR

Gene	Forward Primer (5'-3')	Reverse Primer (5'-3')
FincoR	TCCTAGGTCTTTGACCTTCCAA	TGTGCCCACTGGTGAAATAG
Non-specific region	GTGTACACGCCCAAACTTGA	GTTCACCTCTCTAGCTCACCT

1153

1154 D. List of primer used for RACE

	Gene specific primer (5'-3')
5'RACE	GATTACGCCAAGCTT GGGAACTCACGTCTGGAAGCAGAAGCTG
3'RACE	GATTACGCCAAGCTT GGACACTCGGGAATTGACAGTGGGTCAGG
3'RACE nest primer	GATTACGCCAAGCTT GTGGGGGATAGCACAAGCGCCAGGATGC

1155

1156 E. List of primer used for genotyping

	Forward Primer (5'-3')	Reverse Primer (5'-3')
	GTGATTTCCTTTCCCACAGC	GTCAGGGAGCTAACGAATGC

1157

Figure 1

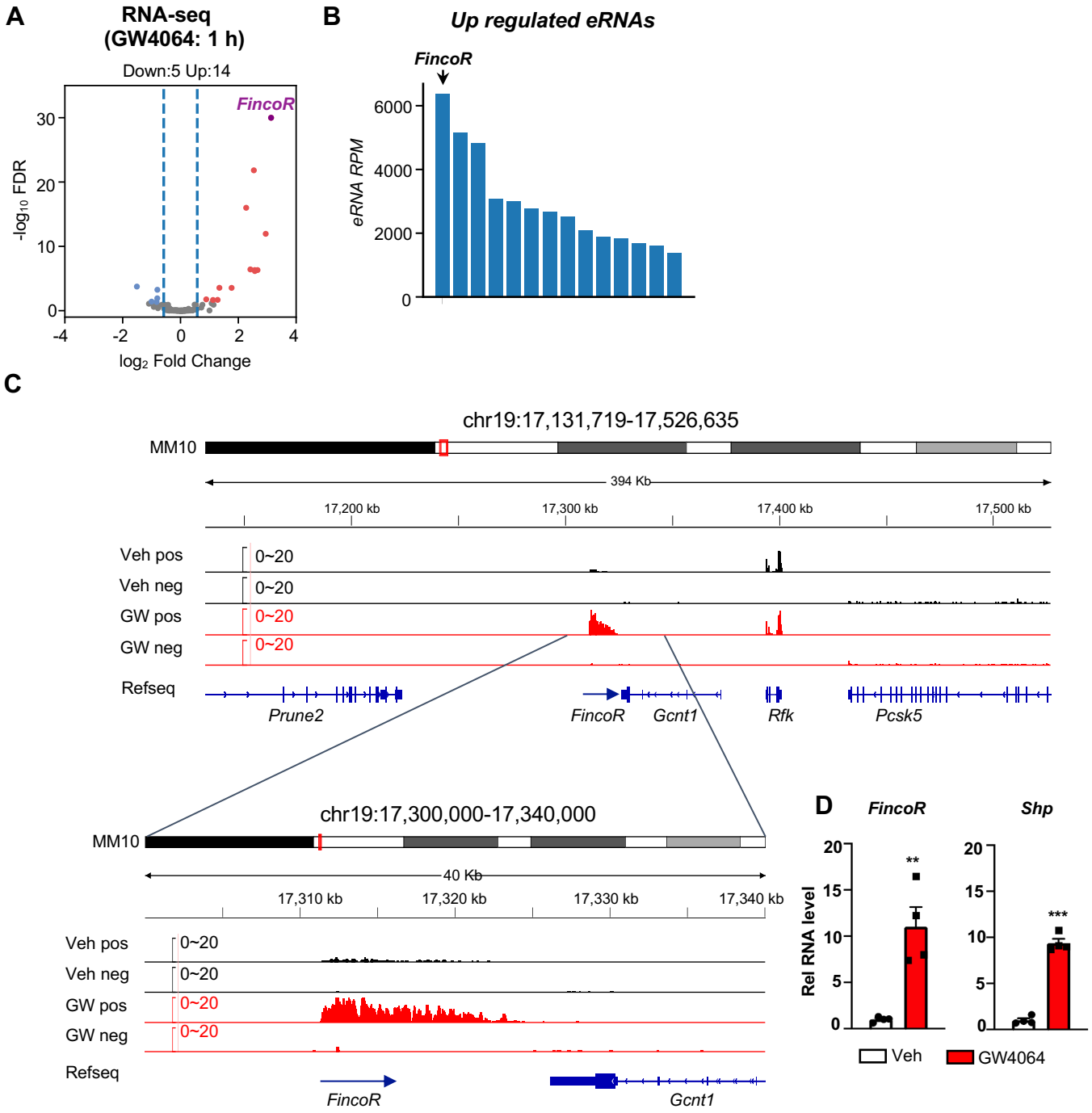
A
RNA-seq
(GW4064: 1 h)
Down:5 Up:14
FincoR
-log10 FDR
log2 Fold Change
B
Up regulated eRNAs
FincoR
eRNA RPM
C
chr19:17,131,719-17,526,635
MM10
394 Kb
17,200 kb
17,300 kb
17,400 kb
17,500 kb
Veh pos
Veh neg
GW pos
GW neg
0~20
Refseq
Prune2
FincoR
Gcnt1
Rfk
Pcsk5
chr19:17,300,000-17,340,000
40 Kb
17,310 kb
17,320 kb
17,330 kb
17,340 kb
D
FincoR
Shp
Rel RNA level
Veh
GW4064

Figure 2

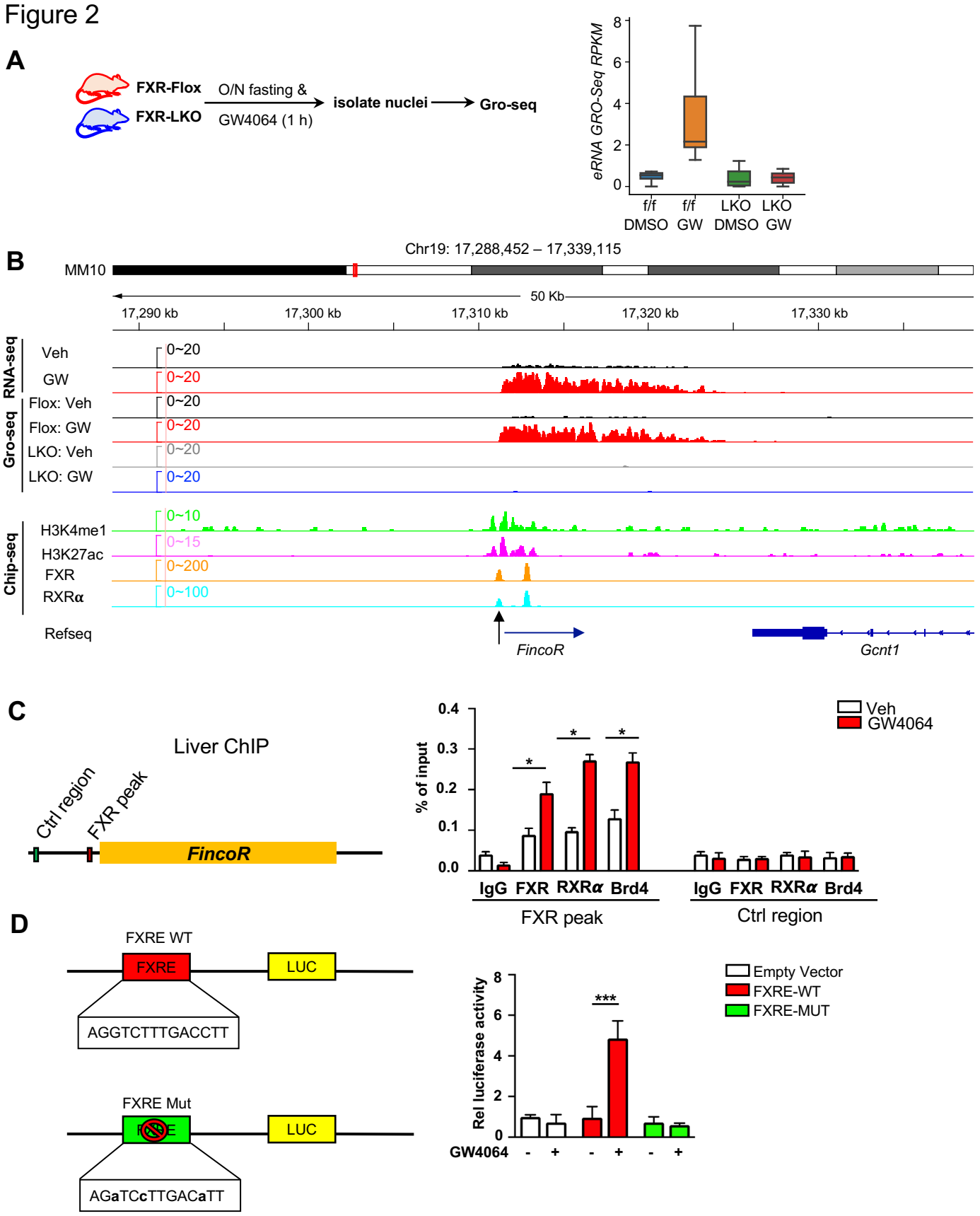
A
FXR-Flox
FXR-LKO
O/N fasting &
GW4064 (1 h)
isolate nuclei
Gro-seq
eRNA GRO-Seq RPKM
f/f DMSO
f/f GW
LKO DMSO
LKO GW
B
Chr19: 17,288,452 – 17,339,115
MM10
50 Kb
17,290 kb
17,300 kb
17,310 kb
17,320 kb
17,330 kb
RNA-seq
Veh
GW
Gro-seq
Flox: Veh
Flox: GW
LKO: Veh
LKO: GW
Chip-seq
H3K4me1
H3K27ac
FXR
RXRα
Refseq
FincoR
Gcnt1
C
Liver ChIP
Ctrl region
FXR peak
FincoR
% of input
Veh
GW4064
IgG FXR RXRα Brd4
FXR peak
Ctrl region
D
FXRE WT
FXRE
LUC
AGGTCTTTGACCTT
FXRE Mut
LUC
AGaTCcTTGACaTT
Rel luciferase activity
Empty Vector
FXRE-WT
FXRE-MUT
GW4064

Figure 3

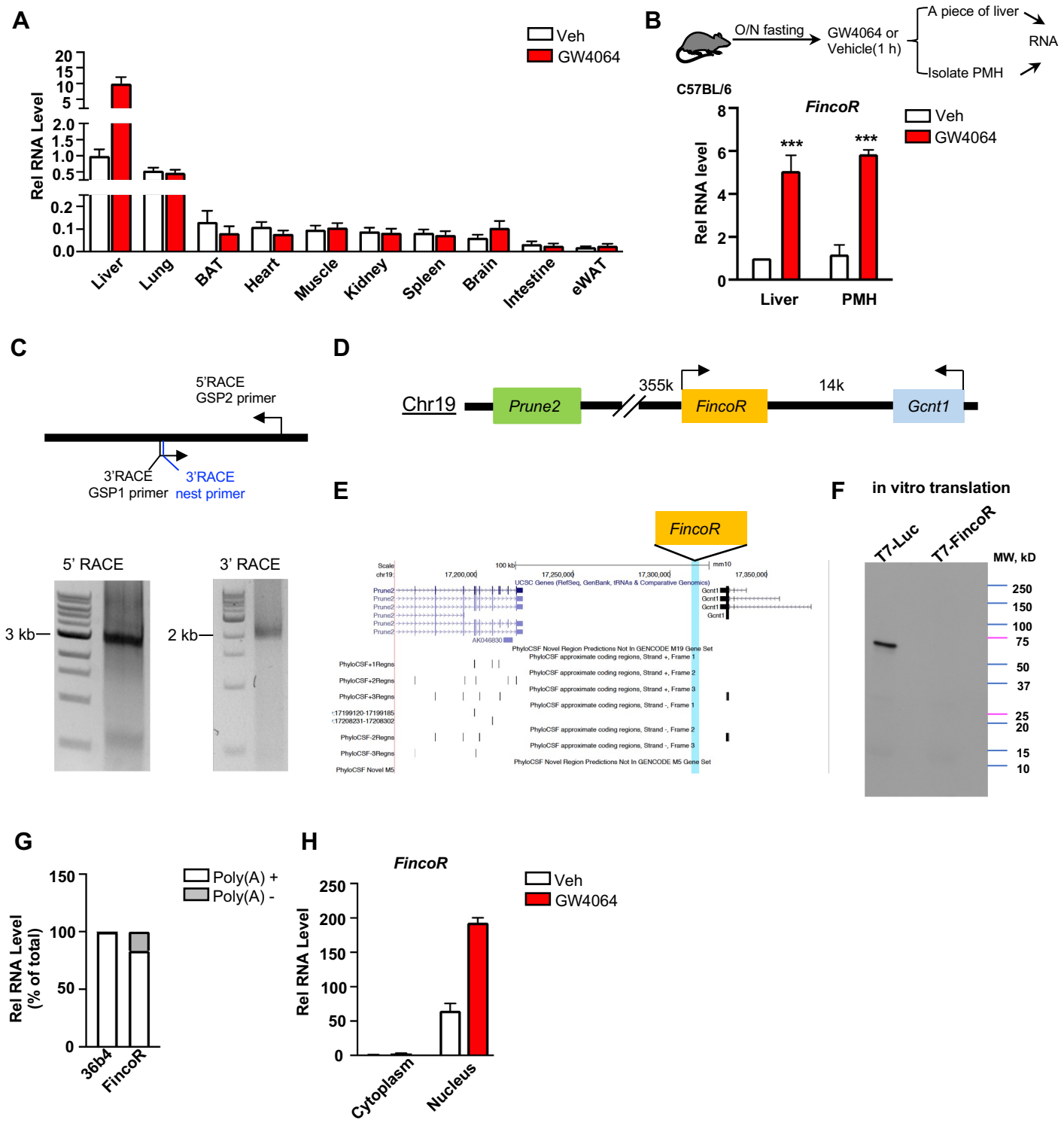
A
Veh
GW4064
Rel RNA Level
20
15
10
5
2.0
1.5
1.0
0.5
0.2
0.1
0.0
Liver
Lung
BAT
Heart
Muscle
Kidney
Spleen
Brain
Intestine
eWAT
B
O/N fasting
GW4064 or Vehicle(1 h)
A piece of liver
RNA
Isolate PMH
C57BL/6
FincoR
Veh
GW4064
Rel RNA level
***
***
Liver
PMH
C
5'RACE GSP2 primer
3'RACE GSP1 primer
3'RACE nest primer
5' RACE
3' RACE
3 kb
2 kb
D
Chr19
Prune2
355k
FincoR
14k
Gcnt1
E
FincoR
F
in vitro translation
T7-Luc
T7-FincoR
MW, kD
250
150
100
75
50
37
25
20
15
10
G
Poly(A) +
Poly(A) -
Rel RNA Level (% of total)
150
100
50
0
36b4
FincoR
H
FincoR
Veh
GW4064
Rel RNA Level
250
200
150
100
50
0
Cytoplasm
Nucleus

Figure 4

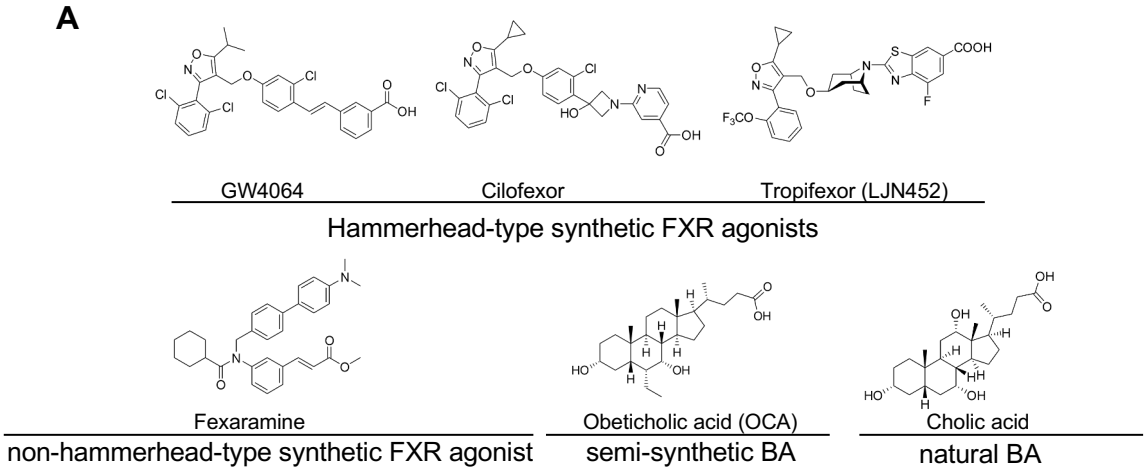
A
GW4064
Cilofexor
Tropifexor (LJN452)
Hammerhead-type synthetic FXR agonists
Fexaramine
non-hammerhead-type synthetic FXR agonist
Obeticholic acid (OCA)
semi-synthetic BA
Cholic acid
natural BA

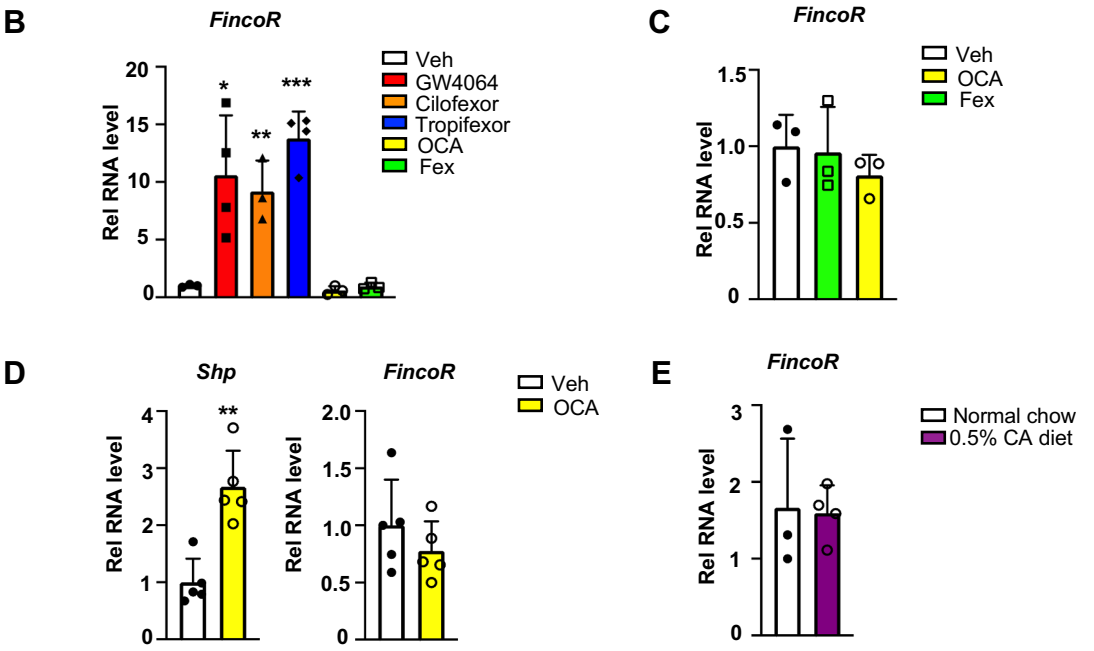
B
FincoR
Rel RNA level
Veh
GW4064
Cilofexor
Tropifexor
OCA
Fex
C
FincoR
Rel RNA level
Veh
OCA
Fex
D
Shp
FincoR
Rel RNA level
Veh
OCA
E
FincoR
Rel RNA level
Normal chow
0.5% CA diet

Figure 5

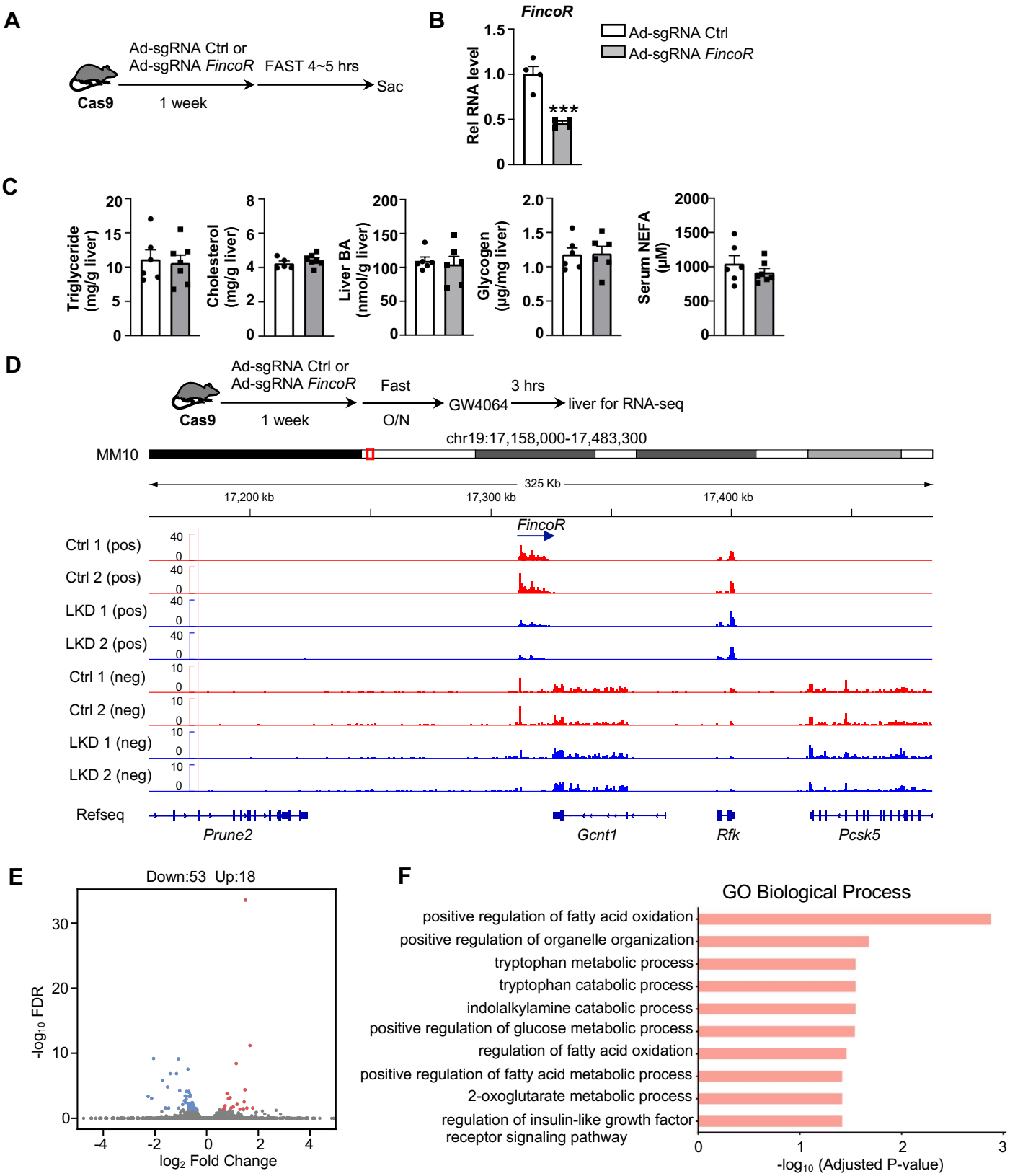
A
Ad-sgRNA Ctrl or
Ad-sgRNA FincoR
FAST 4~5 hrs
Sac
Cas9
1 week
B
FincoR
Rel RNA level
Ad-sgRNA Ctrl
Ad-sgRNA FincoR
***
C
Triglyceride (mg/g liver)
Cholesterol (mg/g liver)
Liver BA (nmol/g liver)
Glycogen (µg/mg liver)
Serum NEFA (µM)
D
Ad-sgRNA Ctrl or
Ad-sgRNA FincoR
Fast
3 hrs
Cas9
1 week
O/N
GW4064
liver for RNA-seq
MM10
chr19:17,158,000-17,483,300
325 Kb
17,200 kb
17,300 kb
17,400 kb
FincoR
Ctrl 1 (pos)
Ctrl 2 (pos)
LKD 1 (pos)
LKD 2 (pos)
Ctrl 1 (neg)
Ctrl 2 (neg)
LKD 1 (neg)
LKD 2 (neg)
Refseq
Prune2
Gcnt1
Rfk
Pcsk5
E
Down:53 Up:18
-log10 FDR
log2 Fold Change
F
GO Biological Process
positive regulation of fatty acid oxidation
positive regulation of organelle organization
tryptophan metabolic process
tryptophan catabolic process
indolalkylamine catabolic process
positive regulation of glucose metabolic process
regulation of fatty acid oxidation
positive regulation of fatty acid metabolic process
2-oxoglutarate metabolic process
regulation of insulin-like growth factor receptor signaling pathway
-log10 (Adjusted P-value)

Figure 6

Ad-sgRNA Ctrl + Veh | Ad-sgRNA Ctrl + Tropifexor | Ad-sgRNA *FincoR* + Tropifexor

A

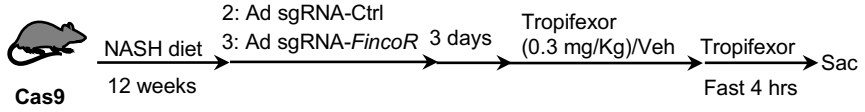

B

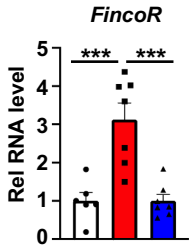

C

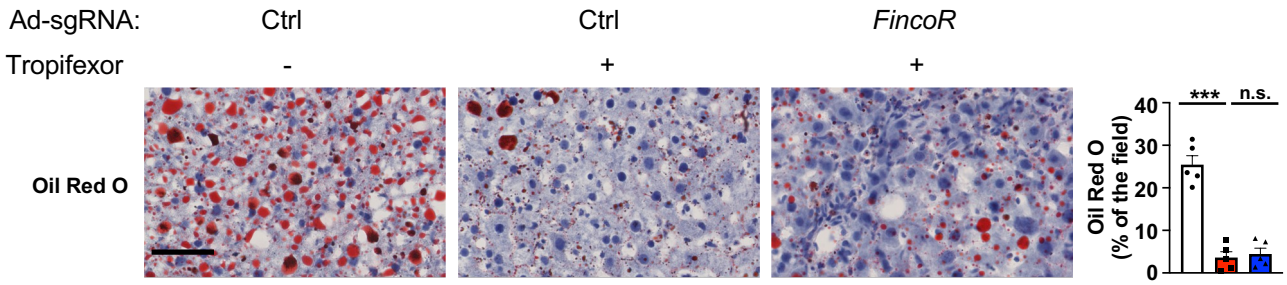

D

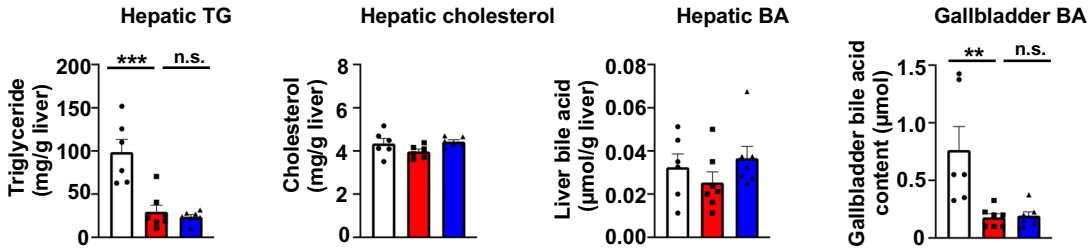

E

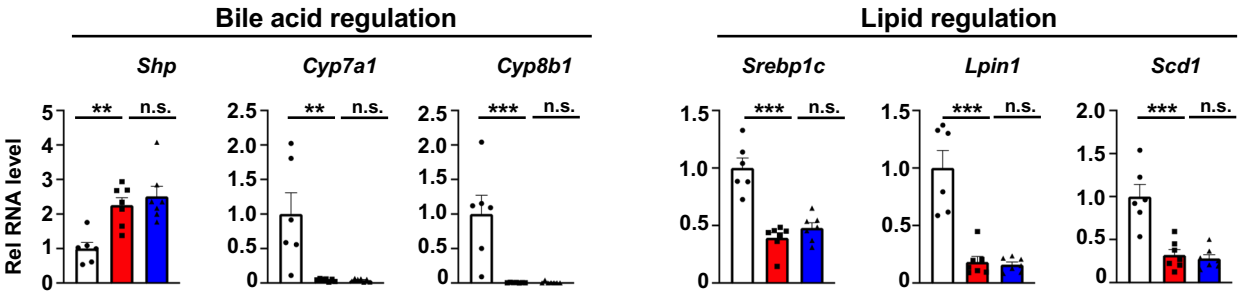

Ad-sgRNA Ctrl + Veh | Ad-sgRNA Ctrl + Tropifexor | Ad-sgRNA *FincoR* + Tropifexor

Figure 7

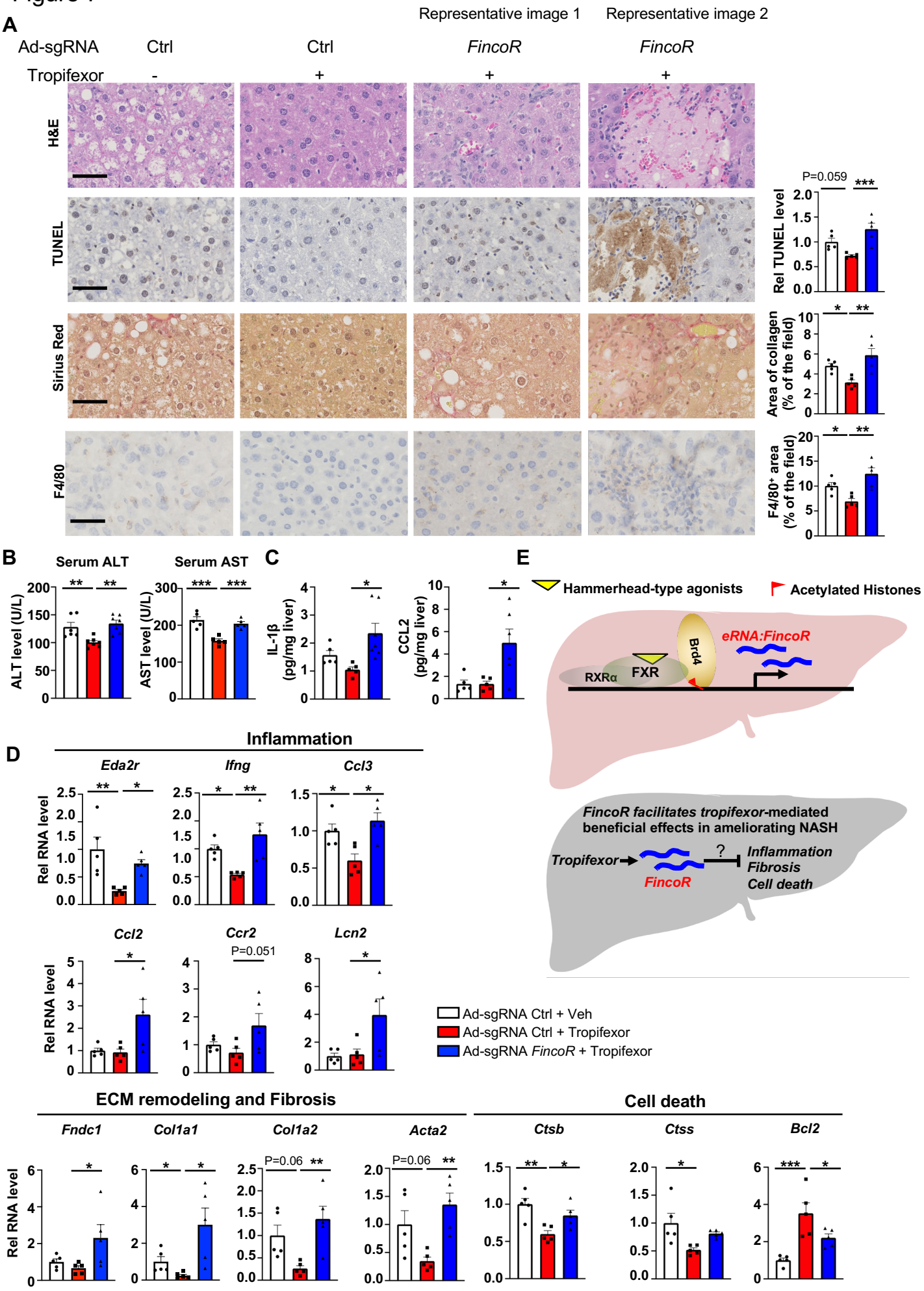
A
Representative image 1
Representative image 2
Ad-sgRNA
Ctrl
Ctrl
FincoR
FincoR
Tropifexor
-
+
+
+
H&E
TUNEL
Sirius Red
F4/80
P=0.059
Rel TUNEL level
Area of collagen (% of the field)
F4/80+ area (% of the field)
B
Serum ALT
Serum AST
ALT level (U/L)
AST level (U/L)
C
IL-1β (pg/mg liver)
CCL2 (pg/mg liver)
E
Hammerhead-type agonists
Acetylated Histones
eRNA:FincoR
Brd4
FXR
RXRα
FincoR facilitates tropifexor-mediated beneficial effects in ameliorating NASH
Tropifexor
FincoR
?
Inflammation
Fibrosis
Cell death
D
Inflammation
Eda2r
Ifng
Ccl3
Ccl2
Ccr2
Lcn2
P=0.051
Rel RNA level
Ad-sgRNA Ctrl + Veh
Ad-sgRNA Ctrl + Tropifexor
Ad-sgRNA FincoR + Tropifexor
ECM remodeling and Fibrosis
Cell death
Fndc1
Col1a1
Col1a2
Acta2
Ctsb
Ctss
Bcl2
P=0.06

Figure 1-figure supplement 1

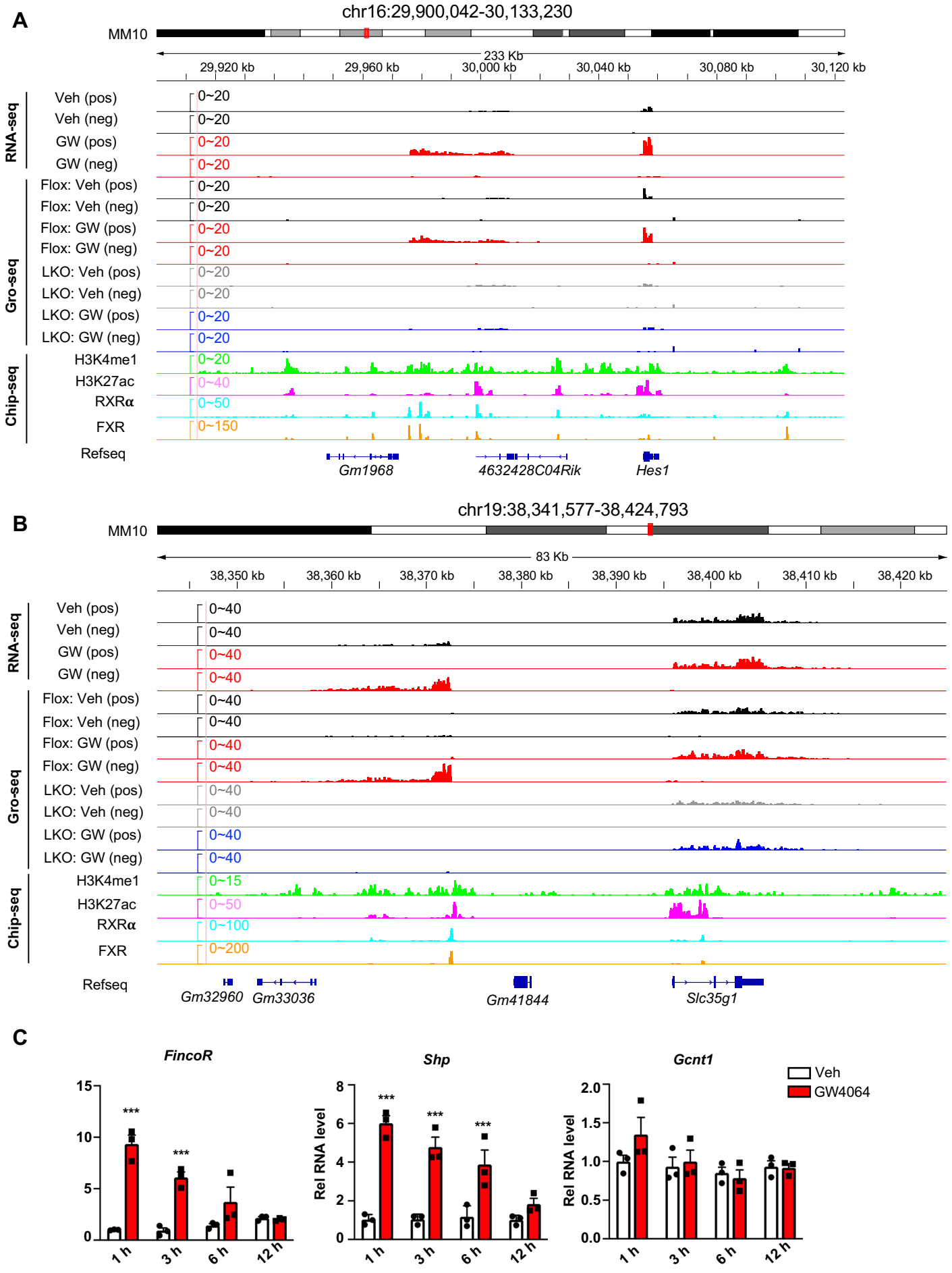

Figure 1–figure supplement 2

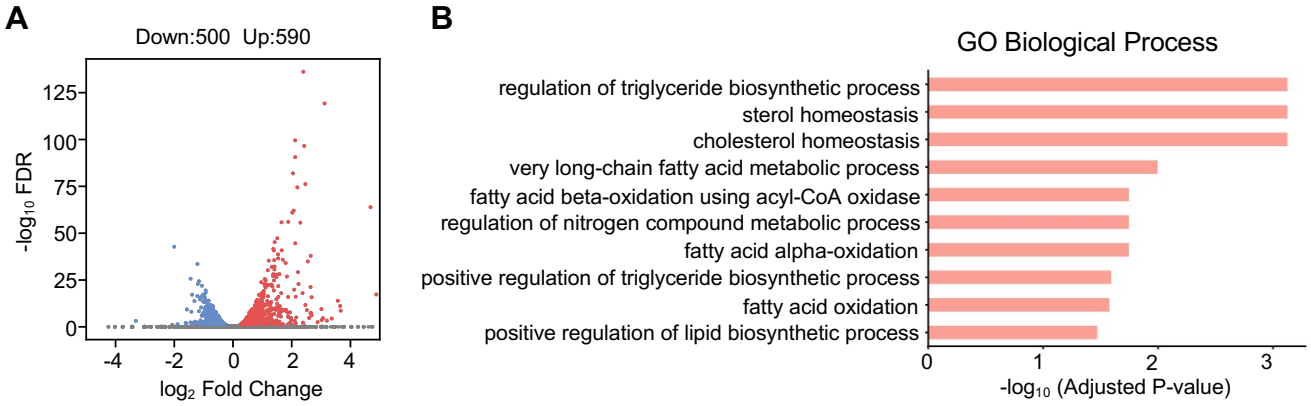

Figure 2-figure supplement 1

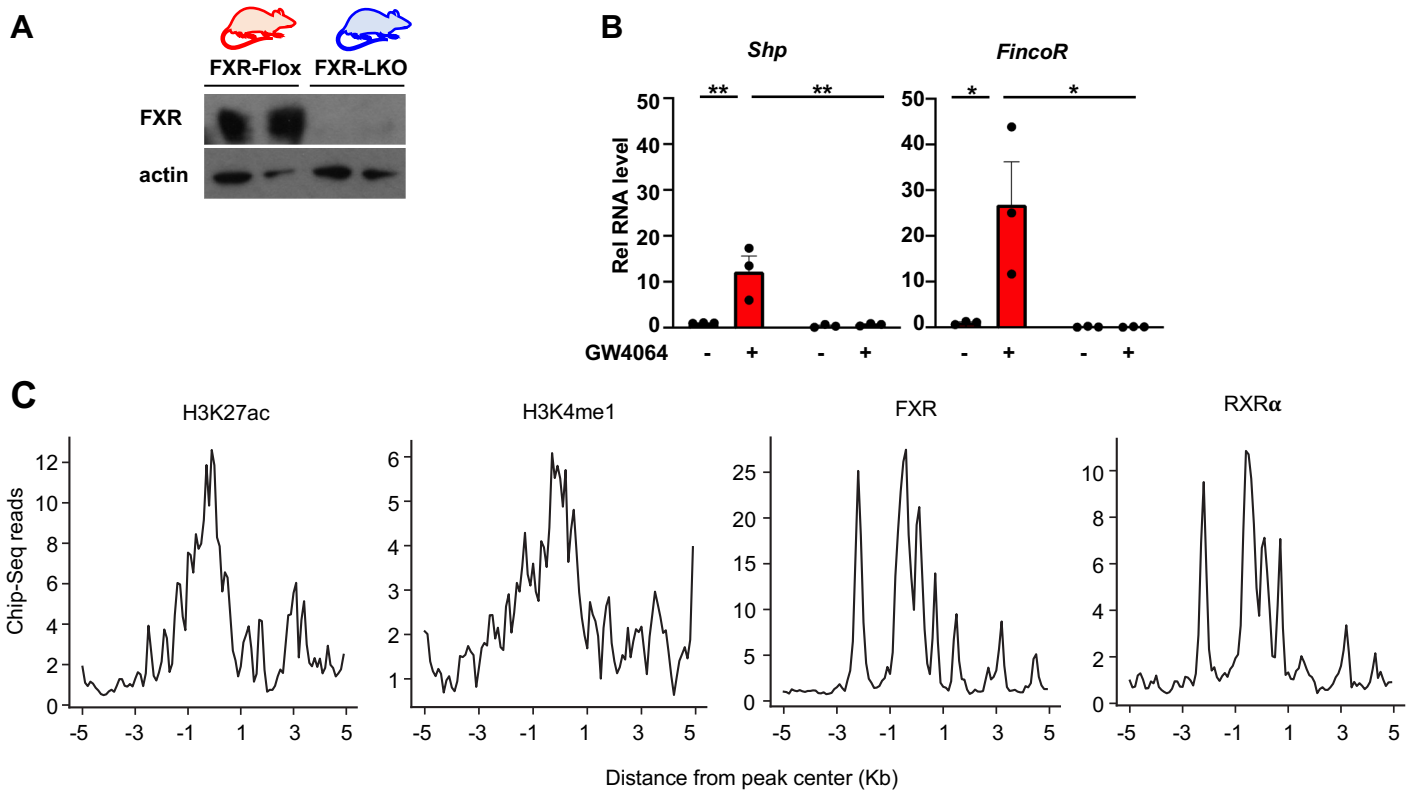

Figure 5-figure supplement 1

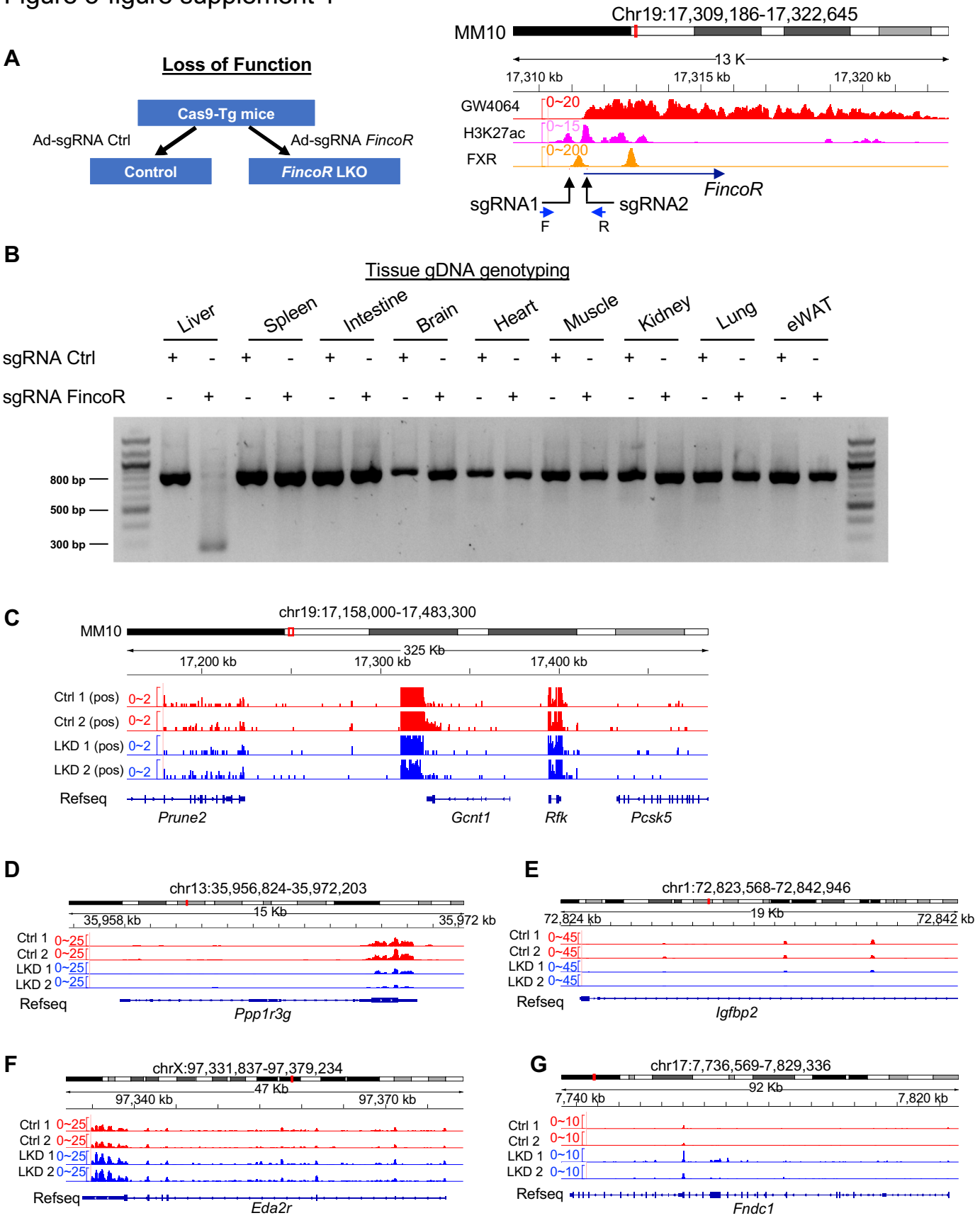

Figure 7-figure supplement 1

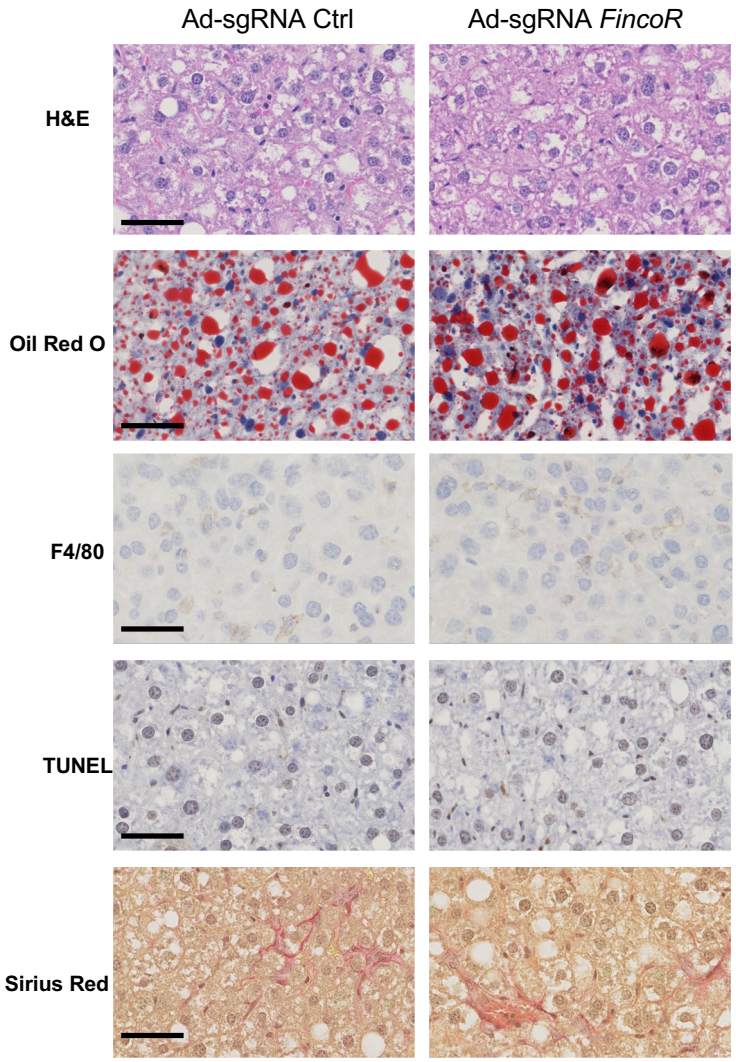

Supplementary Figure S1

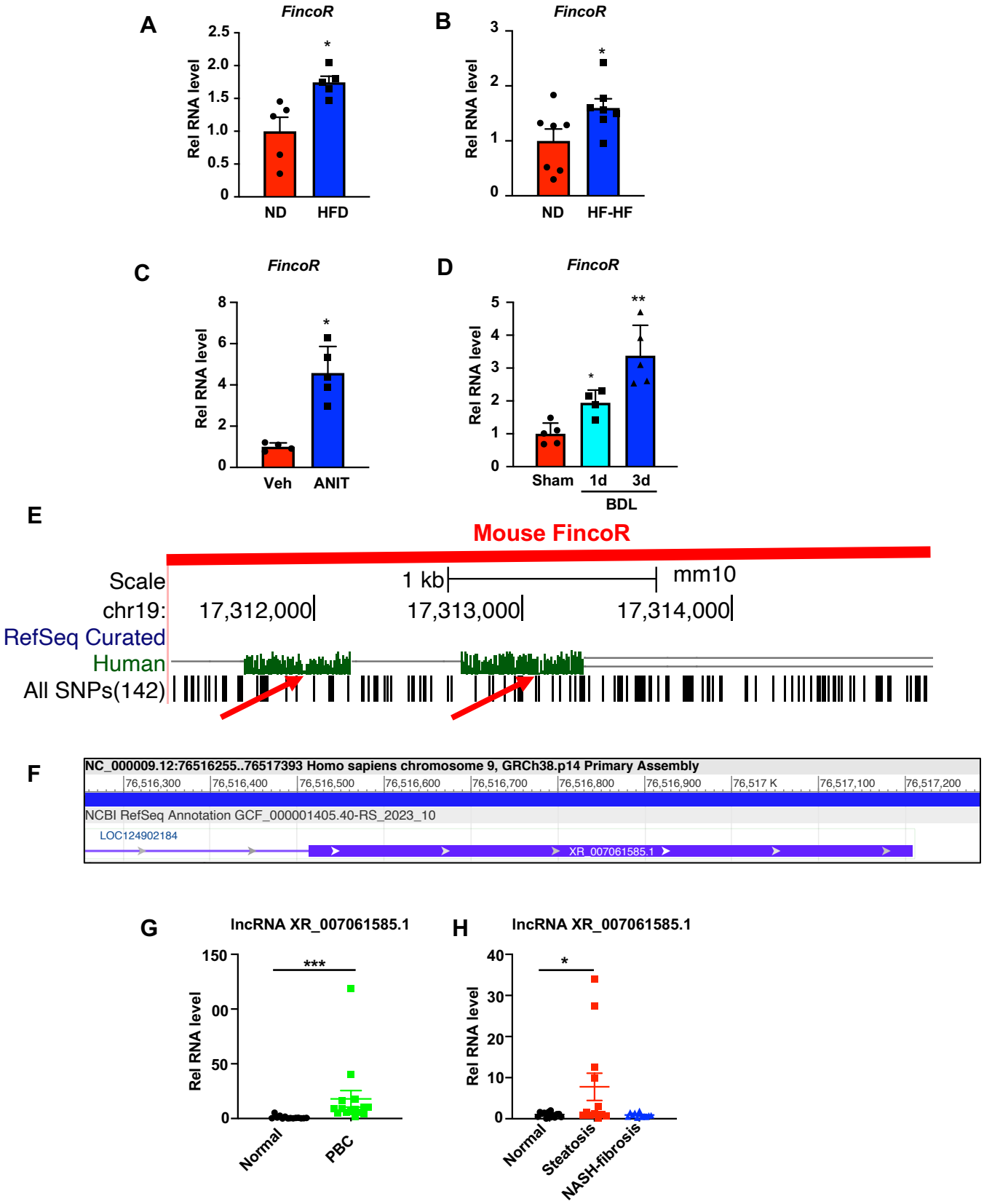

Supplementary Figure S2

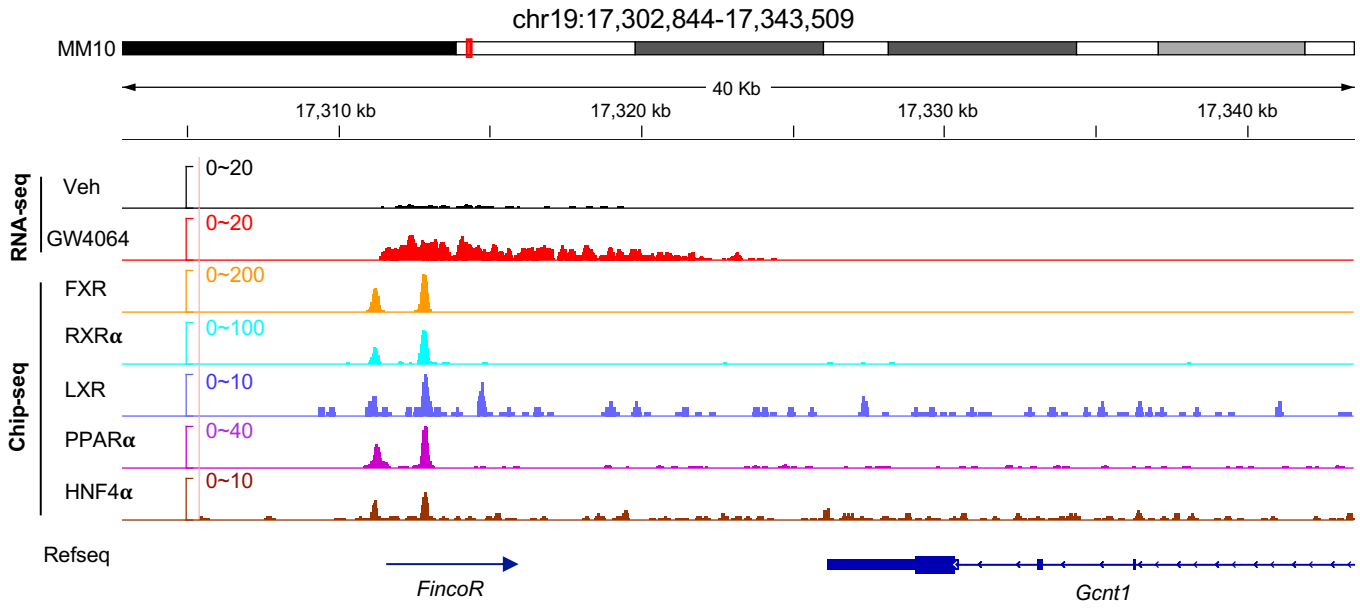
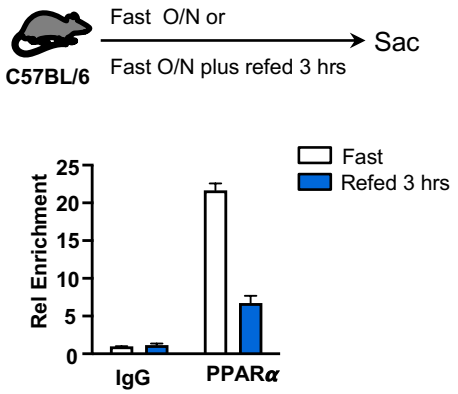
Supplementary Figure S3